Available online at www.sciencedirect.com

SCIENCE DIRECT®

Journal of Volcanology and Geothermal Research 135 (2004) 169–193

Journal of volcanology and geothermal research

www.elsevier.com/locate/jvolgeores

Surface unit characterization of the Mauna Ulu flow field, Kilauea Volcano, Hawai′i, using integrated field and remote sensing analyses

Jeffrey M. Byrnes[a,*], Michael S. Ramsey[a], David A. Crown[a,b]

[a] *Department of Geology and Planetary Science, University of Pittsburgh, Pittsburgh, PA 15260-3332, USA*
[b] *Planetary Science Institute, Tucson, AZ 85719-23951, USA*

Accepted 5 December 2003

Abstract

Investigation of surface units in the Mauna Ulu flow field, Kilauea Volcano, Hawai′i, was conducted through field and remote sensing analyses. Recently acquired Advanced Spaceborne Thermal Emission and Reflection Radiometer (ASTER) and MASTER (MODIS/ASTER airborne simulator) datasets, which cover the visible- through thermal-wavelength region, have been analyzed and correlated with a field-based characterization of Mauna Ulu flow-unit surfaces. Field observations were made of unit morphologies (decimeter- to decameter-scale) as well as small-scale (millimeter- to centimeter-scale) surface textures. Estimates were made of the extent of surface crust spallation, as well as the abundance of vesicles and phenocrysts on the surface crust and spallation surfaces. The field-based characteristics were compared with remote sensing data, including visible and near-infrared reflectance spectra, thermal infrared emissivity spectra, and emissivity-derived small-scale roughness. Visible-wavelength characteristics are controlled primarily by color, luster, and decimeter- to meter-scale surface irregularities, whereas thermal-wavelength characteristics are primarily controlled by the abundance of small-scale roughness elements such as vesicles. Although individual data pixels are not of sufficient resolution to identify typical individual lava flow units using point spectra, mean spectra allow characterization of unit surface crusts. Flow-unit morphologies and surface textures are related to differences in emplacement and post-emplacement modification of ′a′a and pahoehoe lobes. Pahoehoe surface properties reflect the flow regime during emplacement and the history of cooling, degassing, and crystal formation/settling. The nature of pahoehoe surface crusts indicates that within the wide range of emplacement conditions expressed within the flow field, two sets of conditions are dominant, producing a bronzy, smooth crust or a dark, rough crust. The former makes up the majority of the pahoehoe surfaces and reflects minimal cooling and degassing prior to emplacement, whereas the latter reflects cooling and crystallization during storage within the flow field. This study provides a detailed characterization of Mauna Ulu surface units, and presents an integrated field and remote sensing approach to mapping and interpreting the emplacement of lava flow fields.

Keywords: volcanism; remote sensing; lava flows; pahoehoe; Mauna Ulu; Hawai′i

1. Introduction

Knowledge of lava flow emplacement processes is fundamental to characterizing volcano growth and to

* Corresponding author. Tel.: +1-412-624-8773; fax: +1-412-624-3914.
E-mail address: byrnes@ivis.eps.pitt.edu (J.M. Byrnes).

0377-0273/$ - see front matter © 2004 Elsevier B.V. All rights reserved.
doi:10.1016/j.jvolgeores.2003.12.016

understanding the development of lava flow fields on Earth and in other planetary environments. The objectives of this research are to quantitatively characterize surfaces within the Mauna Ulu lava flow field, Kilauea Volcano, Hawai′i (Fig. 1), to document relationships between surface units and remote sensing signatures, and to use the distribution of surface units to examine flow field development using remote sensing analyses. Field observations were made to determine surface characteristics associated with different types of lava flow units, to identify which characteristics related to flow emplacement can be identified remotely, and to provide a ground-based comparison to the remote sensing data. Remote sensing analyses utilized recently acquired Advanced Spaceborne Thermal Emission and Reflection Radiometer (ASTER) and MASTER (MODIS/ASTER airborne simulator) datasets (Yamaguchi et al., 1998; Hook et al., 2001). These datasets provide a means to extend the spatial and spectral coverage to almost the entire ~ 61 km^2 Mauna Ulu flow field from an initial ~ 6 km^2 study site within the flow field, which was originally investigated to determine relationships between pahoehoe surface units, topography, and lava tubes (Byrnes and Crown, 2001). The current study also further develops a field and remote sensing approach to mapping and interpreting the emplacement of complex volcanic surfaces.

2. Background

Compound basaltic flow fields are emplaced in a complicated sequence of interfingering and overlapping lava flows. This results in complex surfaces composed of numerous flow units emplaced in different styles and at different times during flow field evolution. The small-scale (millimeter- to centimeter-scale) texture and unit-scale (decimeter- to decameter-scale) morphology of flow surfaces are indicative of local emplacement conditions and provide important constraints for understanding flow field development. For example, surface characteristics have been related to effusion rate (Walker, 1972; Pinkerton and Sparks, 1976; Rowland and Walker, 1990), style of eruption and lava transport (Swanson, 1973), flow rheology (Peterson and Tilling, 1980; Rowland and Walker, 1987), flow inflation (Walker, 1991; Hon et al., 1994), thermal conditions (Keszthelyi and Denlinger, 1996), local topography and lava storage (Crown and Baloga, 1999; Byrnes and Crown, 2001), and scale dependencies of lava distributary networks (Crown et al., 1998, 1999, 2001, 2004).

Swanson (1973) described three gradational pahoehoe types within the Mauna Ulu flow field. Differences in eruption, transport, and degassing are reflected in the morphology and surface texture of these pahoehoe flow types. Near-vent surface-fed flows formed either smooth-surfaced, dense pahoehoe or shelly pahoehoe, depending on whether the lava was emplaced from high lava fountains or overflows of the vent, respectively. Dense, near-vent pahoehoe was fountain-fed, which allowed degassing and produced relatively vesicle-free lava in thin flow units. These flows commonly formed broad, leveed channels with associated overflows that, except for their lack of tumuli, are grossly similar to hummocky tube-fed pahoehoe. Surface units fed from non-fountaining vent overflows were gas rich and produced shelly pahoehoe, which contains cavities formed by volatile exsolution and/or draining of the flow interior. These flows were emplaced as toes and sheets with crusts that may display fractures, buckles, and festoons. Dense, hummocky, tube-fed pahoehoe in the medial and distal portions of the flow field has an intermediate vesicularity indicative of limited degassing during transport through the lava tube system. These flow units have smooth and commonly glassy surfaces, commonly form lobes of pahoehoe toes, and display tumuli. Both fountain-fed and tube-fed flows undergo the transition to ′a′a in various places within the Mauna Ulu flow field (Swanson, 1973).

In addition to a range of meter-scale surface morphologies, differences in small-scale texture have been described. Wilmoth and Walker (1993) characterized differences in vesicles for tube-fed flows in the Mauna Ulu and Kupaianaha flow fields. S-type (spongy) pahoehoe displays selvages (outer ~ 6 cm) containing abundant (>40 vol.%), small (<4 mm), approximately spherical vesicles. P-type (pipe-vesicle bearing) pahoehoe is less common and displays lower vesicularity, lower porosity, and larger vesicles (including pipe vesicles near the base of each flow unit) relative to S-type pahoehoe. P-type pahoehoe may also be distinguished in young basalt flows based upon its distinct bluish surface coloration. S-type

pahoehoe commonly spalls flakes of the surface skin (millimeter-scale thickness) during and immediately following emplacement, whereas spallation is negligible for P-type pahoehoe. Wilmoth and Walker (1993) suggest that spallation of S-type crust occurs due to focusing of thermal-contraction stresses within the vesicular selvage that does not occur within the dense P-type crust.

Vesicles are significant for several reasons in addition to their effect of increasing bulk flow viscosity (e.g. Polacci et al., 1999). The distribution of vesicles is indicative of pahoehoe eruption and transport styles, as described above for fountain- vs. vent overflow-fed and surface- vs. tube-fed pahoehoe flows (Swanson, 1973). Vesicles also affect flow cooling, as increased surface vesicle abundance promotes cooling of flow lobes (Keszthelyi and Denlinger, 1996; Harris et al., 1998). Furthermore, vesicle distributions are correlated with flow ponding, coalescence, and inflation, reflecting the local pressure and cooling conditions at the interface of a flow's surface crust and molten interior (Hon et al., 1994; Cashman and Kauahikaua, 1997).

3. The Mauna Ulu flow field

The Mauna Ulu satellitic shield is located on the upper east rift zone of Kilauea Volcano (Fig. 1). An approximately 61-km^2 flow field was emplaced from Mauna Ulu and local vents in two main episodes. The long-lived eruption (May 1969 to July 1974) displayed a wide variety of activity, including fire-fountaining (up to >500 m high), ''gas-piston'' cycles of lava column rise and fall, and the development of an extensive lava tube system that fed flows more than 12 km from the vent region to the Pacific Ocean (Swanson, 1973; Swanson et al., 1979; Tilling et al., 1987).

Holcomb (1976) mapped the distribution of ′a′a as well as surface-fed and tube-fed pahoehoe within the Mauna Ulu flow field. He indicated that tube-fed pahoehoe flows emanated from ''master lava tube systems'' that are marked by low, broad ridges. Swanson (1973) suggested that most of the Mauna Ulu tube-fed pahoehoe was probably emplaced from small, distributary tubes that branched from the master tubes.

4. Field characterization of the Mauna Ulu flow field

4.1. Initial Mauna Ulu site study

The Mauna Ulu flow field was chosen because the flows are well exposed and relatively pristine (mostly free of soil and vegetation), and because the eruption was long lived and well documented (e.g. Moore et al., 1973; Swanson, 1973; Holcomb, 1976, 1987; Swanson et al., 1979; Tilling et al., 1987). In addition, the Mauna Ulu flow field has been imaged by a variety of remote sensing instruments at multiple wavelengths. An initial site within the Mauna Ulu flow field (Byrnes and Crown, 2001) was selected to examine the diversity of pahoehoe surface units; this site is within flows that were mapped by Holcomb (1976) as tube-fed flows and classified as dense, hummocky pahoehoe by Swanson (1973). The initial study site is located on and below Holei Pali 7 to 9 km from the Mauna Ulu vent and covers ~ 6.2 km^2 (~ 10% of the flow field). Four varieties of pahoehoe lava flow surface units were defined and mapped using high-resolution color aerial photographs (Byrnes and Crown, 2001). Field observations indicated that the visible-wavelength signatures represented in the photographs are controlled by the characteristic colors, surface textures (roughness and presence or lack of glassy crust), and morphologies (sheets, toes, or channels) of these units.

The four pahoehoe units mapped in the initial study area display primary morphologies related to their emplacement. These morphologies range from sheets (broad, flat units occurring where emplacement is unconfined, or resulting from the coalescence and inflation of toes and/or small sheets and channels) to toes (small units, interconnected networks of which form small to intermediate lobes) to channels (centralized area of flow concentration, occurring where local flow rates are sufficiently high) (Byrnes and Crown, 2001). Flow-unit surfaces may be smooth, ropy, or slabby, gradational to a clinkery ′a′a texture. Unit I is characterized by highly reflective, bronze-colored sheets that display little decimeter-scale topography, large occurrences of which display composite surfaces containing coalesced small sheets and/or toes. Unit II is composed of lobes of pahoehoe toes that display a similar crust and preserve decimeter-

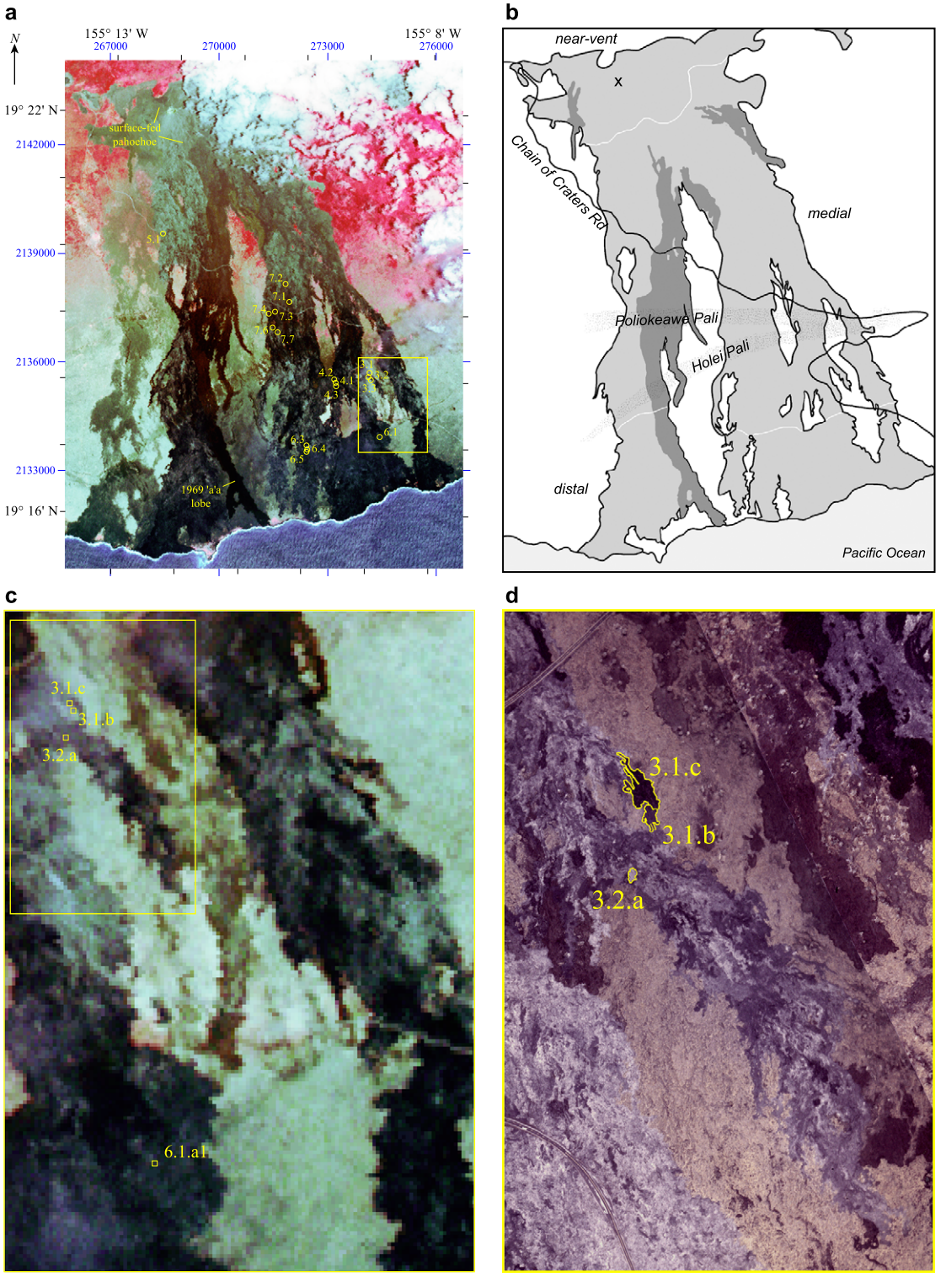
a
N
155° 13' W
267000
270000
273000
155° 8' W
276000
19° 22' N
2142000
2139000
2136000
2133000
19° 16' N
surface-fed pahoehoe
1969 'a'a lobe
b
near-vent
x
Chain of Craters Rd
medial
Poliokeawe Pali
Holei Pali
distal
Pacific Ocean
c
3.1.c
3.1.b
3.2.a
6.1.a1
d
3.1.c
3.1.b
3.2.a

scale toe topography, and is transitional to unit I with increased flow coalescence and inflation. Although unit I and II have similar surface crusts, examination of which is a focus of the current study, they are distinguished based on their primary morphology, either sheet (unit I) or toe network (unit II). Unit III is composed of lobes of dark pahoehoe toes that lack a smooth, reflective surface crust, appears to have had a higher flow viscosity during emplacement (based on relatively equant toes and vesicles preserved on exposure surfaces), and represents locally late-stage emplacement (based upon stratigraphic position, and consistent with inferred viscosity). Unit IV typically exhibits a disrupted, slabby surface that includes primary unit I, II, and III surfaces and is transitional to ′a′a. Unit IV is commonly found in channelized zones that may be bordered by lateral levees. Byrnes and Crown (2001) provide detailed descriptions and field photographs of these units.

The surface unit distribution was found to be correlated with pre-eruption topography and position within the flow field (i.e. along lateral flow field margins vs. within lobe interiors away from the margins) (Byrnes and Crown, 2001). Units were not found to be spatially correlated with the main feeder lava tubes mapped by Holcomb (1976), consistent with the assessment of Swanson (1973) that lava was emplaced primarily from distributary tubes rather than master tube segments. Recent field mapping (Crown et al., 2001, 2004) indicates that the Mauna Ulu lava tube network is more complex than is shown by Holcomb (1976), which is consistent with mapping of active lava tubes within the Pu′u ′O′ o-Kupaianaha flow field (Mattox et al., 1993; Kauahikaua et al., in press) and suggests that Holcomb's mapping was not sufficiently detailed to accurately represent tube system geometry. Small-scale textures of surface crusts were found not to be directly coupled to unit morphology, and field analyses indicate that the semi-quantitative classification of visible-wavelength images does not reflect transitional forms observed between the four tube-fed pahoehoe units defined in the initial study (Byrnes and Crown, 2001). In order to further characterize Mauna Ulu surface units, the current study has three objectives: (1) to identify relationships between small-scale surface textures and flow morphologies to allow further discrimination of surface units, based on detailed field analyses of pahoehoe surface crusts; (2) to incorporate thermal infrared (TIR) remote sensing analyses to complement visible-wavelength analyses, because TIR data is influenced by textural and compositional variations; and (3) to extend the spatial coverage from the initial study area in order to incorporate additional types of surface units for analyses of flow field development.

4.2. Methodology

In the current study, field observations were made over a large portion of the flow field in order to describe the variety of surface units within the Mauna Ulu flow field, document surface parameters related to flow emplacement, and identify which parameters may produce identifiable visible- and thermal-wavelength spectral signatures. Based on these observations and the remote sensing coverage, specific sites were selected that represent typical unit exposures as well as the range of morphologies and surface textures observed, including transitions between units. Areas where anthropogenic activity appeared to have affected unit surface characteristics were avoided in the site selection process. The selected study sites range in size from ~ 7 to 3000 m^2 and include 15 exposures of unit I, 9 exposures of unit II, and 7 exposures of unit III

Fig. 1. Mauna Ulu flow field. (a) ASTER image, with band 3 (0.81 μm) as red, band 2 (0.66 μm) as green, and band 1 (0.56 μm) as blue. The proximal region is dominated by surface-fed pahoehoe flows, the medial region is composed of ′a′a and tube-fed pahoehoe, and the distal region is on the coastal plain where tumuli are prominent. Dense vegetation on the pre-Mauna Ulu surface of Kilauea Volcano appears red in the composite image. UTM (zone 5) data projection uses WGS84 spheroid. Locations of study sites, based on dGPS data, are indicated in yellow (cf. Table A1). Clouds appear white to cyan and are visible in the northeast portion of the image, obscuring part of the near-vent region. Box shows location of c. (b) Sketch map indicating extents of Mauna Ulu flow field. Approximate boundaries of near-vent (proximal), medial, and distal portions of the flow field are indicated by white lines. Also illustrated are the Mauna Ulu vent (X), portions of Poliokeawe and Holei Pali that cross the flow field (stippled), some of the larger ′a′a lobes (dark gray), and Chain of Craters Road. (c) Enlargement of ASTER data shows location of pixels from which point spectra were obtained (Section 6, Fig. 12). Box shows location of d. (d) Portion of high-resolution color aerial photograph mosaic illustrating margins of sites 3.1.b, 3.1.c, and 3.2.a and their context within the flow field. Mauna Ulu basalts appear as shades of gray, indicative of units' colors and morphologies (Byrnes and Crown, 2001). Pre-Mauna Ulu basalts appear as shades of brown.

Table 1
Field estimates of small-scale surface characteristics

Site	Crust spalled (%)	Vesicles				Phenocrysts			
		Surface crust		Spallation surface		Surface crust		Spallation surface	
		Abundance (%)	Size (mm)	Abundance (%)	Size (mm)	Abundance (%)	Size (mm)	Abundance (%)	Size (mm)
Unit I									
3.1.d	10	0	–	20	<0.5–3	0	–	<5	≤4
3.2.a	5	0	–	25	<0.5–3	0	–	<1	≤3
3.2.b[a]	90	0	–	30	1–3	0	–	15–20	1
3.3.a	5	0	–	10	1	0	–	<5	1.5
4.1.c	5	0	–	10	<0.5–3	0	–	0	–
4.3.b	40	<5	2	60	<0.5–33	0	–	10	1–2.5
6.1.a	60	0	–	40	0.5–2	0	–	0	–
6.3.a	20	0	–	<5	<1–2	0	–	0	–
6.4.a	70	0	–	40	0.5–2	0	–	0	–
6.5.a	80	10	1–2	40	0.5–2	0	–	<5	1
7.1.aA	<5	0	–	–	–	0	–	–	–
7.2.a	10	0	–	20	1–3	0	–	0	–
7.3.a	10	0	–	30	1–2	0	–	0	–
7.4.a	10	0	–	20	1–2	0	–	<1	2
7.6.a	20	0	–	10	0.5–2	0	–	0	–
Mean[b]	29 ± 26	1 ± 1	–	26 ± 12	–	0	–	3 ± 3	–
Range	<5–90	0–10	1–2	<5–60	<0.5–33	0	–	0–20	1–4
Unit II									
3.1.a	20	0	–	55	0.5–5	0	–	5	<1–5
4.1.b	50	0	–	20	1	0	–	10	≤3
5.1.a	20	0	–	50	0.5–1	0	–	0	–
6.1.a1	50	<5	1–2	30	1–2	0	–	0	–
7.1.aC	20	0	–	20	1	0	–	0	–
7.2.a1	70	0	–	40	0.5–3	0	–	0	–
7.4.a1	50	5	1–2	40	1–4	0	–	20	1–3
7.6.a1	10	0	–	20	0.5–3	0	–	0	–
7.7.a	10	0	–	20	0.5–4	0	–	0	–
Mean[b]	33 ± 19	1 ± 1	–	33 ± 12	–	0	–	4 ± 5	–
Range	10–70	0–5	1–2	20–55	0.5–5	0	–	0–20	<1–5
Unit III									
3.1.b	90	40	1–2	60	<1–5	<5	≤3	10	≤2
4.1.a[c]	80	<5	<5–30	40	1–40	0	–	10	≤5
4.2.a	80	<5	2	40	0.5–2.5	0	–	20	1–4
4.2.b	90	10	1–2	30	2	0	–	<5	<1
5.1.b[d]	70	20	1–13	30	1–3	0	–	20	2–4
7.1.aB	40	70	1–10	50	1–2	0	–	<5	≤4
7.3.a1	–	20	1–2.5	40	1–3	0	–	20	3–10
Mean[b]	75 ± 13	24 ± 18	–	41 ± 8	–	0 ± 1	–	12 ± 7	–
Range	40–90	<5–70	1–30	30–60	0.5–40	<1–<5	≤3	<5–20	<1–10

[a] Unit I exposure at site 3.2.b displays a ropy, channelized sheet surface (rather than the more typical flat sheet surface).

[b] Mean reported as average ± standard deviation; for purposes of calculating standard deviation, <5 is considered 2.5 and <1 is considered 0.5.

[c] Two populations of vesicles are present on site 4.1.a spallation surface, one with small (~ 1 mm) undeformed vesicles and the other with highly deformed vesicles up to 5 mm wide × 40 mm long.

[d] A breakout of higher viscosity lava at site 5.1.b displays spallation surfaces with 20% vesicles (2–3 mm) and 30% phenocrysts (3–7 mm).

(Table 1), which were geolocated using a high-resolution (~ 10 cm horizontal accuracy) differential Global Positioning System receiver (dGPS; Fig. 1, Appendix A). Descriptions of each site were compiled, noting unit morphology and color, context within the flow field and local stratigraphic relationships, topographic characteristics, and small-scale characteristics such as vesicularity, phenocryst abundance, and microtopography. For exposures of units I–III, estimates were made of the degree of spallation of flow-unit surfaces (expressed as the areal percentage of spalled vs. intact crust), and the areal abundance and size of vesicles and phenocrysts on surface crusts and spallation surfaces. The degree of spallation for units I–III was estimated over the entire unit exposure at a given site. Vesicularity and phenocryst abundance and size were estimated by selecting and describing representative areas (typically 5–10% of the unit exposure) of the surface crust and spallation surfaces. These estimates were made in order to characterize the range of surfaces observed and understand gradations between unit surfaces. Values for unit IV and ′a′a surfaces were not obtained. Unit IV surfaces are highly variable, containing slabs that are interpreted to have formed initially as other units and subsequently to have been disrupted, representing a transitional phase to the development of ′a′a clinkers. ′A′a surfaces do not typically preserve any quenched, glassy crust, and vesicularity estimates are not possible on these surfaces. Qualitative comparisons, however, were made to near-vent (fountain-fed and shelly), P-type, and unit IV pahoehoe varieties, as well as ′a′a.

4.3. Results

Morphologically, unit I exposures at the decimeter- to meter-scale typically are flat or display ropy, channelized zones and range from individual sheets to composite surfaces composed of coalesced toes and sheets. The unit exhibits the lowest mean degree of crust spallation (29%; Table 1), although also is characterized by a wide range in this value. Surface crusts display limited (< 5%), small (1–2 mm) vesicles and no phenocrysts, tend to be bronzy and glassy, and may be smooth or display mm-size ridges or dark, glassy knobs. Unit I spallation surfaces display more and larger vesicles than non-spalled crust, some small phenocrysts, and are concentrated in areas within the unit that have undergone deformation due to surface folding during emplacement or local post-emplacement inflation. Two types of surface coatings or alteration have been observed at some locales: (1) a white variety spatially associated with small cracks, possibly gypsum; and (2) a splotchy, yellow to orange variety that appears to be preferentially associated with pahoehoe ropes but is also found in flat parts of exposures, which is likely palagonite (e.g. Crisp et al., 1990; McBirney, 1993). The areal extent of observed alterations and coatings varies within individual exposures of a unit and between adjacent units, but is typically minimal.

Unit II exposures consist of lobes of toe networks that display a similar low mean degree of crust spallation (33%; Table 1) and exhibit both smooth surfaces and small, ropy, channelized zones. Similar to unit I, unit II surface crusts display limited (< 5%), small (1–2 mm) vesicles and no phenocrysts, tend to be bronzy and glassy, and may be smooth or display millimeter-scale ridges and/or dark, glassy knobs. Spallation surfaces are commonly more vesicular than those of unit I and exhibit phenocrysts, and are also associated with disrupted areas. Both the white and splotchy surface coatings/alteration have been observed on unit II surfaces.

Unit III exposures consist of lobes of toe networks that may be smooth (at the decimeter-scale), ropy, or slabby. Toes tend to be more equant, lobes are thicker, and crust spallation is more prevalent relative to toes of unit II. Unit III is generally the last unit emplaced locally, based on flow stratigraphy, and is fed as breakouts from other surface units. Unit III surface crusts have relatively high vesicularities, may display phenocrysts, and typically are dark and rough (millimeter- to centimeter-scale) due to the presence of glassy knobs and/or ridges. Some unit III exposures feed breakouts of even darker, more viscous lava that typically displays more abundant and larger vesicles and phenocrysts. In limited areas, the unit III surface crust displays rare bronzy glass filaments similar to those that are a common part of unit I and II surface crusts. Spallation surfaces display more and larger vesicles and phenocrysts. The splotchy variety of surficial coating/alteration tends to be orange and is commonly found on pahoehoe ropes.

Unit IV exposures are typically areally extensive and commonly bounded by levees. They display highly disrupted surfaces composed of jumbled plates

and slabs exhibiting textures associated with units I, II, and III that are intermixed with ′a′a clinkers. ′A′a surfaces typically lack glass, may be dark gray to red, and are rough at the millimeter- to decimeter-scale.

Other varieties of pahoehoe were also observed, including surface-fed and transitional units. Both shelly pahoehoe and dense, fountain-fed pahoehoe typically display a bronzy surface crust similar to units I and II (Fig. 2). The fountain-fed pahoehoe units are generally large (Fig. 2a) and display a relatively smooth, bronzy surface crust and a range of morphologies consistent with emplacement as sheets, channels, and large (meter-scale), elongate toes. Shelly pahoehoe displays a similar bronzy appearance, although it is not typically as smooth. Shelly pahoehoe may be emplaced as sheets or toes and is hollow beneath the upper few centimeters, and with collapse of the shelly crust is transitional to a

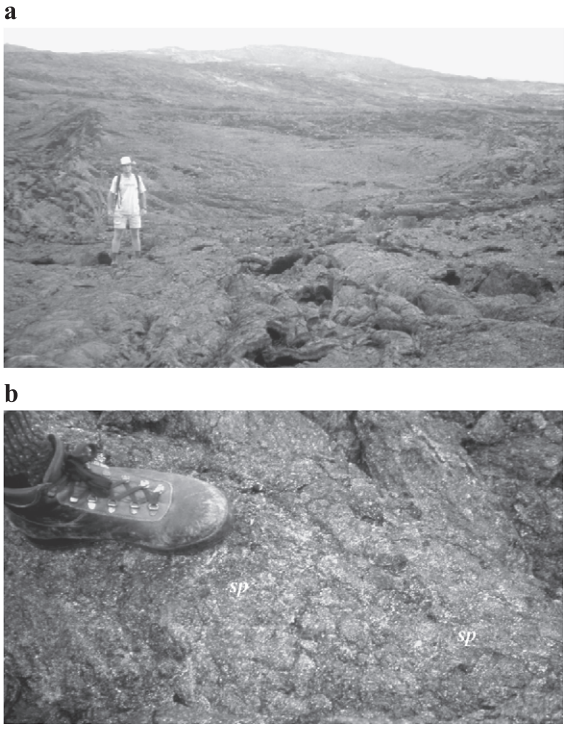

Fig. 2. Surface-fed pahoehoe in the Mauna Ulu proximal region. (a) Overview, showing folded and buckled shelly pahoehoe in the foreground (on which B. Banks is standing), fountain-fed pahoehoe in midground, and Mauna Ulu vent in background. (b) Detail of shelly pahoehoe surface, displaying the altered glassy crust and small portions of the spallation surface (*sp*).

disrupted surface similar to unit IV. Intermediate units that display transitions to both surface-fed varieties were also observed, indicated by Swanson (1973) to have formed from low (< 100 m) lava fountains. The surface-fed flows observed in the proximal region have undergone significant post-emplacement degradation of their surfaces compared to tube-fed flows in the medial and distal regions, presumably due to greater rainfall in the proximal region (~ 3 m at the vent vs. ~ 1 m at the coast; Hawaii Statewide GIS Program data available at http://www.state.hi.us/dbedt/gis/). Those units closest to the vent have additionally been subjected to post-emplacement chemical alteration due to degassing and potentially steam interaction.

Field estimates of spallation, vesicle abundance, and phenocryst abundance are shown in Table 1. Each of the units displays a wide range in the proportion of surface crust that has been spalled and the abundance of vesicles and phenocrysts. The mean areal percent of spalled crust is similar for units I (29%) and II (33%) and significantly higher for unit III (75%). Spallation appears to occur at different scales, from flaking of the outermost skin (millimeter-scale thickness) to fracturing and removal of crust (centimeter-scale thickness), which exposes darker, progressively higher-vesicularity portions of a flow-unit's interior. Most of the vesicles that had formed on the surfaces of units I and II were stretched and flattened due to plastic deformation of the crust during emplacement. Unit III tends to preserve the concave surface expression of vesicles, although vesicles may be deformed. Vesicularity within flow units indicates that units I, II, and III are S-type pahoehoe. Vesicularity estimates were not made for ′a′a surfaces; however, these surfaces were consistently found to have greater millimeter- to centimeter-scale roughness than the pahoehoe units. Olivine is the only phenocryst mineral identified. Phenocryst abundance on the spallation surface (Table 1) is higher within unit III exposures (12%) than for units I (3%) and II (4%).

Transitions between the four tube-fed pahoehoe units are common. Unit I sheets undergo a transition to unit II toes at their margins due to decreased flow rate, and unit II toey lobes undergo a transition to unit I sheets through coalescence and inflation of the flow unit (Byrnes and Crown, 2001). A transitional unit that is intermediate between units I and III is present

in the medial region above Holei Pali. It displays a unit I sheet morphology and a surface texture similar to unit III, attributed to high supply rates relative to typical, toey unit III exposures and a degree of apparent pre-emplacement cooling intermediate to the typical unit I and III end members. Unit I, II, and III morphologies may all change to a unit IV morphology with disruption of the flow surface, commonly associated with increased flow rate and/or inflation and generally manifested as breaking of the unit into slabs. Additionally, units III and IV are transitional to an ′a′a texture with increased disruption of the flow surface.

Our observations indicate that S-type pahoehoe is much more abundant than P-type at Mauna Ulu, consistent with the findings of Wilmoth and Walker (1993). We observed one exposure of P-type pahoehoe below Holei Pali (site 6.2.a, Appendix A), which is similar to descriptions by Wilmoth and Walker (1993). The exposure displays a glassy blue crust that lacks vesicles and phenocrysts and exhibits millimeter-scale knobs and minimal crust spallation (< 5%). The spallation surface contains < 1% vesicles (0.5–1.0 mm). Void spaces observed in the unit interior were few in number, but were large (decimeter scale) and occupied a substantial proportion of the volume of small lobes. The splotchy surface coating/alteration was observed to be extensive on the exposure, and the white ‘‘crack filling’’ variety was also observed.

4.4. Significance

Detailed characterization of pahoehoe surfaces yields a wide range of estimated values of surface spall, vesicle abundance, and phenocryst abundance. This indicates that each of the units may be produced under a variety of conditions, which is consistent with the observed unit transitions. The characterization also indicates, however, that the smooth, bronzy surface crust (units I and II) and the dark, rough surface crust (unit III) represent two primary surface textures that presumably reflect dominant conditions for Mauna Ulu pahoehoe emplacement. Because spallation is related to stresses that develop in the lava crust, the greater amount of unit III spallation and lesser degree of vesicle deformation on exposed unit III spallation surfaces indicates that it had a different thermal history from that of units I and II. Specifically, the exposed surfaces of units I and II were able to plastically deform surface bubbles, producing stretched, flattened vesicles, whereas unit III exposures display vesicles that preserve concavity and exhibit little flow deformation, although brittle deformation of vesicles appears to have occurred. The abundance of vesicles and nature of vesicle deformation are consistent with previous field observations that suggested unit III was relatively viscous during emplacement (Crown and Baloga, 1999; Byrnes and Crown, 2001).

Phenocrysts are indicative of cooling history and may indicate prolonged storage within the subsurface lava tube distributary network or may be transported from the vent. The high phenocryst abundance of unit III (relative to units I and II) contributes to higher bulk flow viscosity (assuming the flow surfaces are representative of the bulk flow, which is suggested by our observations of unit interiors). Furthermore, the abundance of phenocrysts, coupled with the observation that unit III tends to locally be the last emplaced, supports the hypothesis that the lava has experienced storage in the subsurface distributary network (Crown and Baloga, 1999; Byrnes and Crown, 2001). Two mechanisms may produce differences in unit phenocryst content: (1) crystal growth during storage within the flow field; and (2) sorting due to crystal settling. Whereas both processes could contribute to high unit III phenocryst abundance, neither process alone is likely to be efficient enough to produce the observed dichotomy in phenocryst abundance.

Unit IV and ′a′a textures indicate that the flow surface experienced substantial disruption. In this respect, they are secondary textures, although unit IV preserves primary surface crusts on disrupted slabs and plates. Similarities between surface-fed pahoehoe and tube fed units I and II indicate that similar sheet and toe flow regimes occurred throughout the flow field, although several important differences are important for understanding flow field development. The larger areal extent of individual surface-fed toes and sheets suggests that the volumetric supply rate was greater for these units than locally from lava tubes, consistent with observations made of the emplacement of these units (Swanson, 1973). Furthermore, surface-fed flows do not generally appear to have undergone flow inflation, and the significant differences in unit vesicularity (which

affects flow rheology) suggest that the actual emplacement of lava is more varied than is indicated by the resulting morphologies.

These analyses indicate that the various morphologies and textures may form under a range of conditions. For example, toes indicate low local flow rates during emplacement, whereas sheets and channels reflect successively higher flow rates (for similar topography and flow substrate). Field relationships indicate that smooth crusts are associated with flow units (I and II) that were relatively hot and fluid during emplacement, whereas greater areas of spalled vesicular surface are associated with lava that had experienced a greater degree of cooling prior to emplacement (unit III). Combining morphologic and textural information therefore allows better interpretation of the state of the lava during emplacement than either provides by itself. Although the wide range of small-scale characteristics and the transitions between units indicate that the surface units are emplaced under a wide variety of conditions, the type examples suggest that within the range of conditions, a limited set of emplacement conditions (pertaining to supply rate, flow viscosity, cooling history, etc.) were dominant during the development of the Mauna Ulu flow field.

5. Spectral characterization of the Mauna Ulu flow field

5.1. Thermal infrared remote sensing of volcanic surfaces

Thermal infrared (TIR) wavelength remote sensing datasets are useful for mapping variations in surface properties and/or thermal anomalies because thermal radiance is a function of surface emissivity (a material property) and temperature (e.g. Gillespie et al., 1990; Hook et al., 1992; Kahle and Alley, 1992). TIR data have been used to discriminate rocks of different mineralogic content (e.g. Vincent and Thomson, 1972; Walter and Salisbury, 1989) and lithology (e.g. Vincent et al., 1972; Kruse and Kierein-Young, 1990). Previous volcanologic investigations have used TIR data to map the distribution of basaltic units of similar composition and varying age (Kahle et al., 1988), silicic units of similar composition and varying vesicularity (Ondrusek et al., 1993; Ramsey and Fink, 1999), and thermal anomalies associated with active lava tubes (Realmuto et al., 1992).

Because thermal emittance from multiple components mixes linearly in proportion to their areal abundance, TIR spectra can be deconvolved to estimate proportions of end member surfaces within a pixel (Thomson and Salisbury, 1993; Ramsey and Christensen, 1998). Vesicularity variations among flow surfaces of uniform composition can be modeled by measuring the relative depths of spectral features (Ondrusek et al., 1993; Ramsey and Fink, 1997, 1999). For example, a basaltic pahoehoe exposure can be modeled spectrally as a surface composed of smooth basaltic glass and vesicles (or similar small-scale roughness elements). Relative proportions of these two spectral end members are calculated by deconvolving the surface spectrum, linearly fitting the spectral features to mixtures of the end members. The contribution of small-scale roughness elements in effect mutes the glass emissivity features, driving the spectrum towards blackbody behavior (Ramsey and Fink, 1999; Ramsey and Dehn, 2004-this issue). Ramsey and Fink (1999) applied this modeling approach to calculate vesicularity of silicic lava dome surfaces to map the distribution of textural units at Medicine Lake Volcano, California. This methodology is also being applied to active silicic domes (Ramsey and Dehn, 2004-this issue).

5.2. The ASTER and MASTER datasets

Due to the significance of vesicularity for understanding lava flow emplacement, datasets were used in this study that included TIR emittance in addition to visible and near infrared (VNIR) reflectance. These data (Fig. 3) were acquired for the Mauna Ulu flow field by ASTER on May 4, 2000 and by MASTER on October 14, 2000 during the PacRim II mission. The ASTER instrument is described in detail by Yamaguchi et al. (1998), and other applications to understanding volcanic processes are presented by Ramsey and Flynn (2004-this issue) and Pieri and Abrams (2004-this issue). The ASTER data were processed to Level 1B (radiometric and geometric corrections), and have 15 m/pixel spatial resolution in the VNIR, 30 m/pixel in the SWIR, and 90 m/pixel in the TIR. Level 2 data were not available when analyses were conducted. The airborne MASTER instrument was

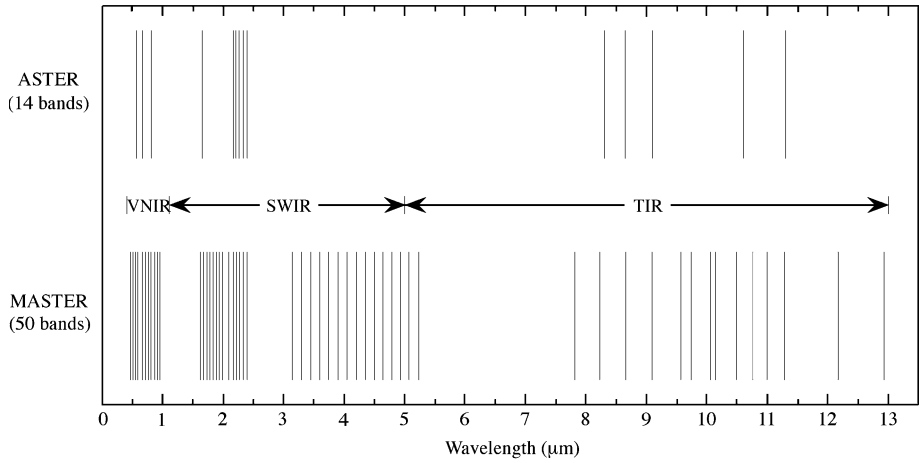

Fig. 3. Band positions of the ASTER and MASTER remote sensing instruments. Wavelength regions indicated: VNIR = visible + near infrared, SWIR = short wavelength infrared, and TIR = thermal infrared.

developed to simulate and validate ASTER and Moderate Resolution Imaging Spectroradiometer (MODIS) data (Hook et al., 2001). The MASTER instrument has an instantaneous field of view of 2.5 mrad for all bands, producing data with ~ 14 m/pixel spatial resolution at nadir at sea level (given a flight altitude of 5458 m).

5.3. Methodology

Remote sensing analyses were performed to determine the spectral characteristics of Mauna Ulu surface units and to assess whether the surface units of interest could be discriminated. First, the ASTER and MASTER datasets were processed as described below, and then mean spectra were derived for identifiable, areally extensive exposures of surface units. These spectra are compared with examples of single pixel spectra in Section 6, and interpretations of the remote sensing images are discussed in Section 7.

ASTER VNIR DN values were converted to ground radiance using the scale factors provided in the dataset header information. A temperature emissivity separation was performed on the ASTER TIR bands in order to remove the temperature component from the ground radiance to yield emissivity. The separation utilized an emissivity normalization technique (Realmuto, 1990) with an emissivity maximum value of 0.985. Moderate variations of the emissivity maximum value do not affect interpretations; Realmuto (1990) indicated that maximum values of 0.95–1.00 are reasonable for basalt, and Kahle and Alley (1992) have shown that small errors in the assumed emissivity value will not affect spectral differentiation. The TIR-derived emissivity values were subsequently normalized to a flat mean water spectrum based on 51,000 pixels (~ 11.5 km^2) representing the Pacific Ocean. This normalization was required to correct for systematic errors that were presumably related to the atmospheric correction. Geometric corrections were applied to the entire ASTER dataset in order to coregister it with the high-precision dGPS data that we collected at Mauna Ulu during November 1999 and July 2001.

The MASTER VNIR DN values were converted to radiance at sensor using the calibration slopes provided in the dataset header information. A standard atmospheric model (MODTRAN) was utilized to convert the radiance at sensor to ground radiance for elevations of 150, 450, and 750 m to account for large-scale differences in atmospheric thickness from sea-level to the vent. This technique models the Mauna Ulu flow field as having three topographic steps, which is more accurate than using a single surface altitude for the entire atmospheric correction. Additionally, a dark-object subtraction was performed on band 1 (0.462 μm) to correct for atmospheric radiance. The TIR MASTER ground radiance was

converted to emissivity (as above) and normalized to a flat mean water spectrum based on 8220 pixels (~ 1.85 km^2) representing the Pacific Ocean. Only MASTER TIR data within the 8- to 12-μm atmospheric window were used. This region is free of H_2O and CO_2 absorptions and contains the strongest reststrahlen bands (fundamental molecular vibrations of silicates) (e.g. Salisbury and D'Aria, 1992).

The data were corrected for panoramic distortion and coregistered with the dGPS and ASTER data. Coregistration of the datasets was performed using nearest neighbor resampling in order to avoid pixel averaging, and all bands in both datasets were resampled to 15 m/pixel. For comparison, a mosaic of high-resolution color aerial photographs of the initial study site and a supervised classification derived from the mosaic (Byrnes and Crown, 2001) were also coregistered with the dGPS, ASTER, and MASTER data.

Average VNIR-derived reflectance and TIR-derived emissivity values were calculated to compare mean spectra of the four pahoehoe surface units of the initial site study (Byrnes and Crown, 2001). The pahoehoe unit map of Byrnes and Crown (2001) was used to create data masks (representing the entire classification) for pahoehoe units I–IV. Mean spectra for those units were calculated using the masks with subsampled, processed ASTER and MASTER datasets. Means represent averages of 1,342,821 pixels (~ 1.34 km^2) for unit I, 778,452 pixels (~ 0.78 km^2) for unit II, 358,367 pixels (~ 0.36 km^2) for unit III, and 304,726 pixels (~ 0.30 km^2) for unit IV in the subsampled data. Average ′a′a spectra are based on the distal portion of an extensive 1969 ′a′a lobe (Fig. 1), using 1190 pixels (~ 0.27 km^2) for ASTER and 2465 pixels (~ 0.55 km^2) for MASTER. Mean spectra for surface-fed pahoehoe (fountain-fed and shelly) were derived from two areas totaling 1404 pixels (~ 0.32 km^2) for ASTER. Fountain-fed and shelly pahoehoe were not analyzed separately in the current study because discrete, extensive exposures of each unit have not been mapped in the available datasets. Surface-fed pahoehoe was not analyzed for MASTER due to extensive cloud cover over the proximal region of the flow field during data acquisition.

Small-scale roughness was calculated for the ASTER and MASTER datasets through application of the linear deconvolution model of Ramsey and Fink (1999). For this study, the model fit two end-member emissivity spectra to each pixel within the datasets, that of an ideal blackbody and a Mauna Ulu basaltic glass sample (laboratory spectra obtained following Ruff et al., 1997). The model then calculated the proportion of each end member to produce a value for each pixel that represents the areal abundance of the blackbody (i.e. small-scale roughness element). The higher MASTER TIR spectral resolution (Fig. 3) provides better constraints on the depth of the 9.1-μm absorption feature.

5.4. Results

Reflectance spectra derived from the ASTER and MASTER VNIR data are shown for the Mauna Ulu surface units in Fig. 4. Error bars representing standard error on the mean are smaller than the symbols used to plot the data, although standard deviations display overlap for all the data plotted. The shapes and magnitudes of the reflectance spectra differ between the two datasets, which may be partly due to atmospheric effects, band positions, and differences in viewing geometry and pixel size. Despite these differences, the flow units display the same overall progression in surface reflectance. Surface-fed pahoehoe displays the greatest reflectance at all wavelengths in the ASTER VNIR (Fig. 4a), and both instruments indicate that reflectance decreases from pahoehoe unit I sheets to unit II toe lobes to unit III breakouts to disrupted unit IV surfaces and finally to ′a′a lobes.

Mean ASTER and MASTER emissivity spectra (Fig. 5) display differences in emissivity at ~ 9.1 μm, which are used with the linear deconvolution model (Ramsey and Fink, 1999) to derive small-scale surface roughness (Fig. 6). Differences in contrast between Fig. 6a and b result from the difference in resolution of the ASTER and MASTER TIR data (90 and >10 m/pixel, respectively). The coarser resolution of ASTER yields pixels that sample more surfaces than MASTER pixels, reducing the range of roughness represented within the flow field. Mean model small-scale roughness values indicate an increase in small-scale surface roughness from relatively smooth-surfaced units I and II to the more highly vesicular unit III to the disrupted unit IV surfaces (Fig. 7), consistent with a previous analysis of Thermal Infrared Multispectral

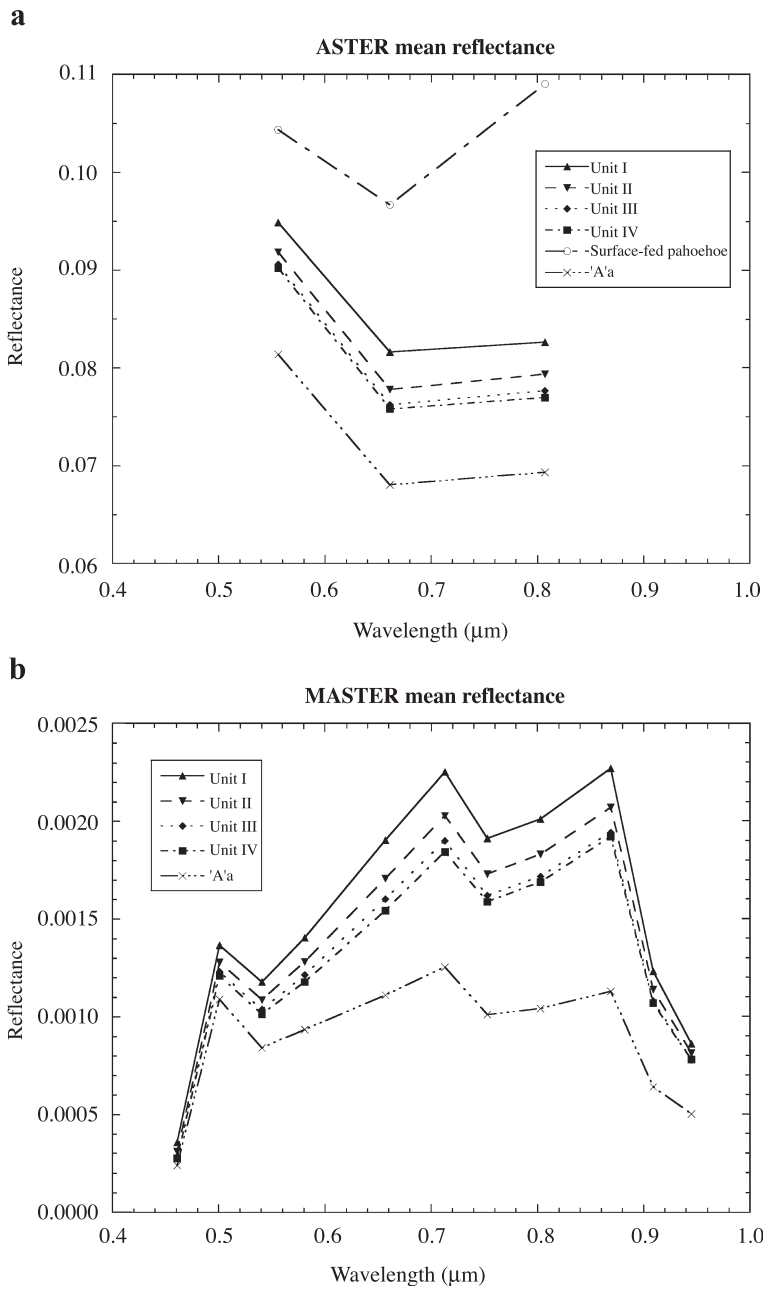

Fig. 4. Mean reflectance spectra for Mauna Ulu surface units, derived from (a) ASTER, bands 1 to 3, and (b) MASTER, bands 1 to 11.

Scanner (TIMS) data (Byrnes et al., 2000). The surface-fed pahoehoe is similar in roughness to unit IV (Fig. 7). ′A′a has the greatest small-scale roughness of the Mauna Ulu surface units (Fig. 7). The range of ′a′a roughness is roughly comparable to that of the pre-Mauna Ulu surface (Fig. 6). Mean emissivity spectra (Fig. 5a) indicate that all pahoehoe units display a pronounced 9.1-μm feature and that the surface-fed pahoehoe differs from the other surface units at ~ 10.7 μm.

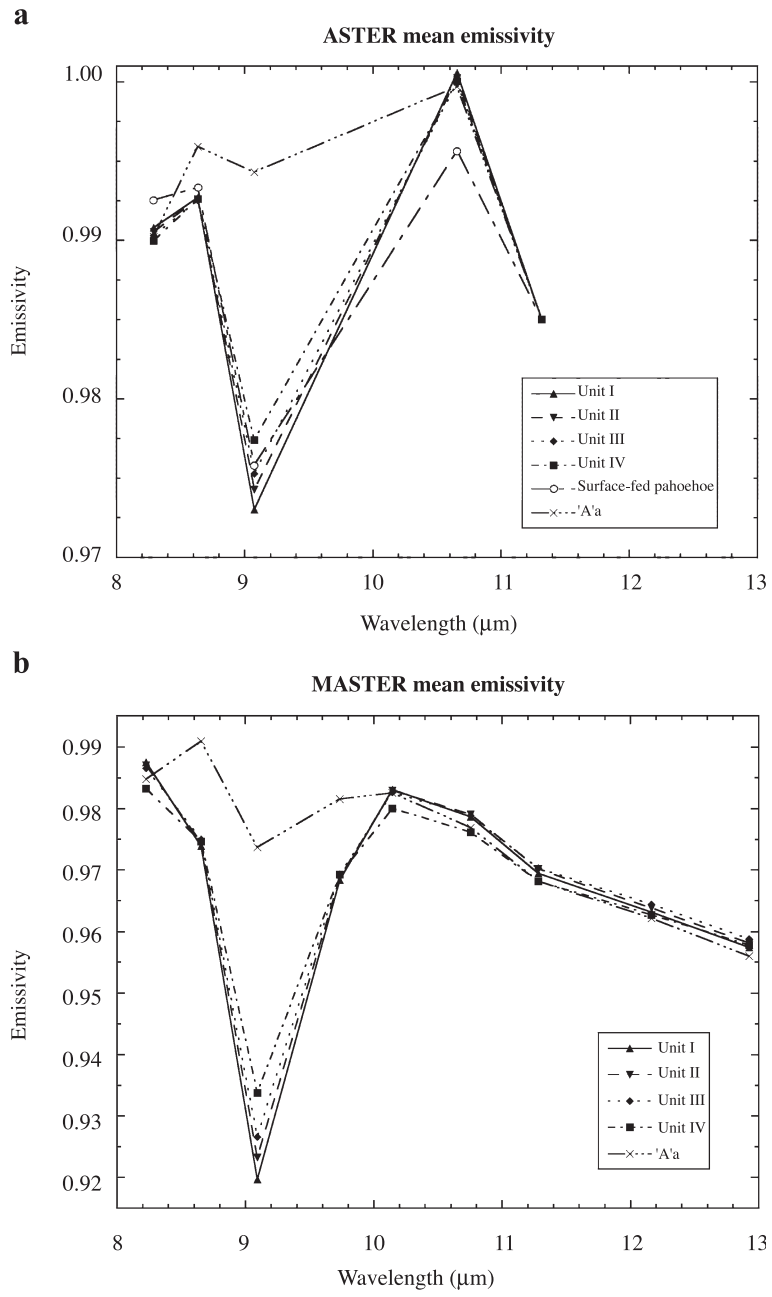

Fig. 5. Mean emissivity spectra for Mauna Ulu surface units, derived from (a) ASTER, bands 10 to 14, and (b) MASTER, bands 42 to 50.

5.5. Significance

The quantitative results presented in Fig. 4 indicate that the surface units can be distinguished on the basis of characteristic surface reflectance. These results are consistent with the qualitative assessments derived from high-resolution color aerial photographs (Byrnes and Crown, 2001) and field observations that indicate

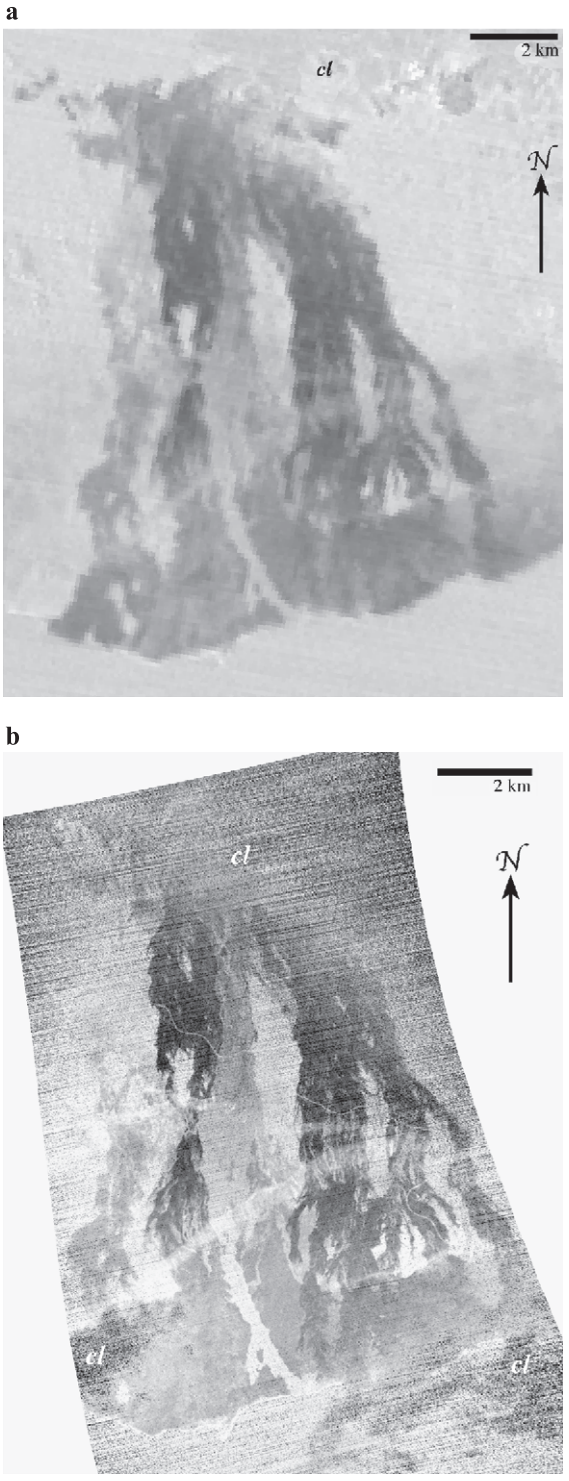

that surface reflectance and color help to distinguish emplacement units defined primarily on the basis of flow morphology.

Mean emissivity spectra (Fig. 5) are consistent with field investigations in this study as well as previous work (Ramsey and Fink, 1997, 1999; Byrnes et al., 2000) that indicates emissivity differences are expected in the surface units due to variations in glass abundance and small-scale roughness. Spectral features associated with the presence of olivine are not identifiable, consistent with field observations of low exposed phenocryst concentrations (Table 1) and the limited areal extent (much less than one 100–8100 m^2 pixel) of the most phenocryst-rich surfaces. An assumption of the temperature-emissivity separation technique is that temperature is isothermal within each pixel. Self-shadowing may be significant for unit IV, shelly pahoehoe, and ′a′a due to the nature of their characteristically irregular surfaces, which may create temperature differences within a pixel and produce errors in derived emissivity (Gillespie et al., 1990). Despite self-shadowing, the results presented herein indicate that the surface units examined have characteristic emissivity spectra that may be used to distinguish them.

The high degree of small-scale roughness for unit IV is interpreted to be due to vesicular flow interiors exposed in disrupted, overturned crust. The high model roughness calculated for the surface-fed pahoehoe may be due to a combination of several factors: increased small-scale roughness associated with collapse of shelly pahoehoe surface crust, depressed emissivity values in ASTER band 13 (~ 10.7 μm; Fig. 5a) that affect the calculated depth of the 9.1-μm glass absorption feature, and enhanced weathering in the proximal region. The high degree of small-scale roughness observed for many pre-Mauna Ulu surfaces reflects a rough, degraded surface, consistent with field observations. The dichotomy between the smooth, bronzy (unit I and II) surface texture and the dark, rough (unit III) surface texture that is clear in

Fig. 6. Emissivity-derived small-scale roughness maps of the Mauna Ulu flow field. (a) ASTER-derived roughness map. (b) MASTER-derived roughness map; the MASTER data have a higher spatial resolution, resulting in greater image contrast. Each grayscale image is displayed as a linear stretch of the proportion of rough (vs. smooth, glassy) surfaces, from black (0% roughness) to white (100%). Cloud cover (*cl*) has low signal-to-noise.

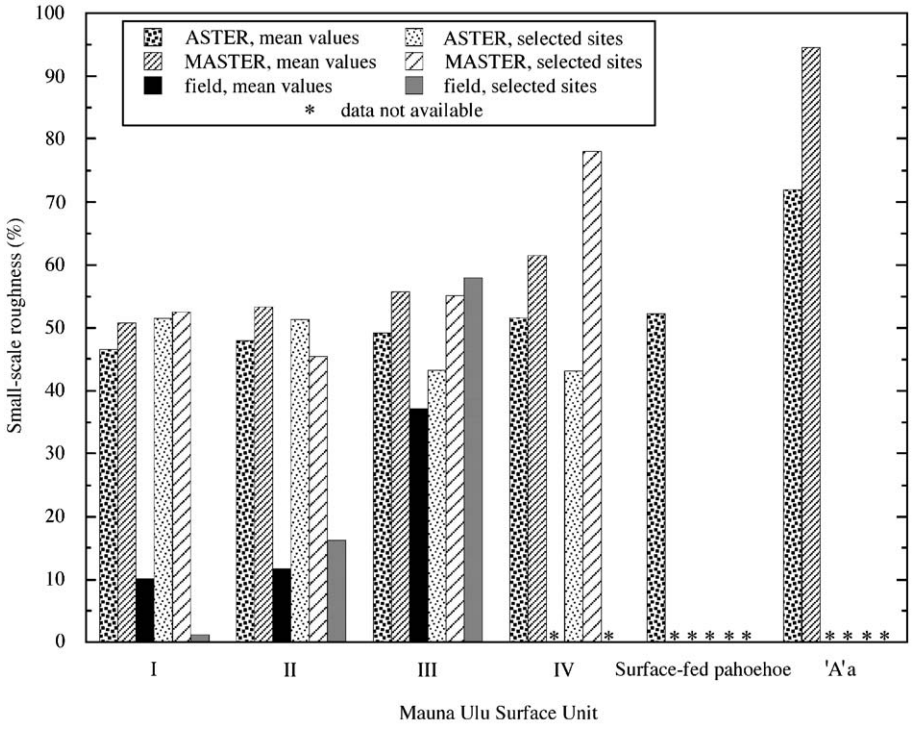

Fig. 7. Small-scale roughness of Mauna Ulu surface units, expressed as a percent of surface area. Mean unit values as well as point values for four selected sites (see Fig. 1 inset and Section 6 text) are compared for field-based vesicularity estimates and emissivity-derived model roughness for ASTER and MASTER. Asterisks indicate data are not available.

field observations is not distinct in the mean VNIR and emissivity spectra. Statistical differences between units I and II in the emissivity data may indicate that unit I displays a lower characteristic degree of crust spallation than unit II, consistent with field data (Table 1). Differences in the VNIR data are attributed to the decimeter-scale morphology (flat sheets vs. undulating toes), consistent with Byrnes and Crown (2001), and may also be related to characteristic differences in the degree of spallation. All pahoehoe units have similar, prominent 9.1-μm absorption features relative to ′a′a (Fig. 5), which produces greater discriminability between the pahoehoe and ′a′a than between the different pahoehoe units (Fig. 6).

6. Field and remote sensing synthesis

Synthesizing field and remote sensing analyses is paramount to applying field observations made at specific study sites to the entire Mauna Ulu flow field, as well as to using remote sensing for investigations of volcanic processes. Four sites were selected based on field data to provide a comparison between tube-fed units I–IV as observed in the field and detected in the remote sensing datasets: site 3.2.a (unit I), site 6.1.a1 (unit II), site 3.1.b (unit III), and site 3.1.c (unit IV). The selected unit I and II examples each display typical unit morphologies as well as complexities due to the transitional nature of the pahoehoe units. The selected unit III and IV sites are the type localities for those units.

6.1. Field descriptions of selected sites

Site 3.2.a (~ 15 × 25 m) is shown in Fig. 8. It exhibits a complex unit I surface composed of coalesced toes and small channels and sheets. The surface crust displays bronze-colored, stretched glass filaments with small (millimeter-scale), dark knobs. In

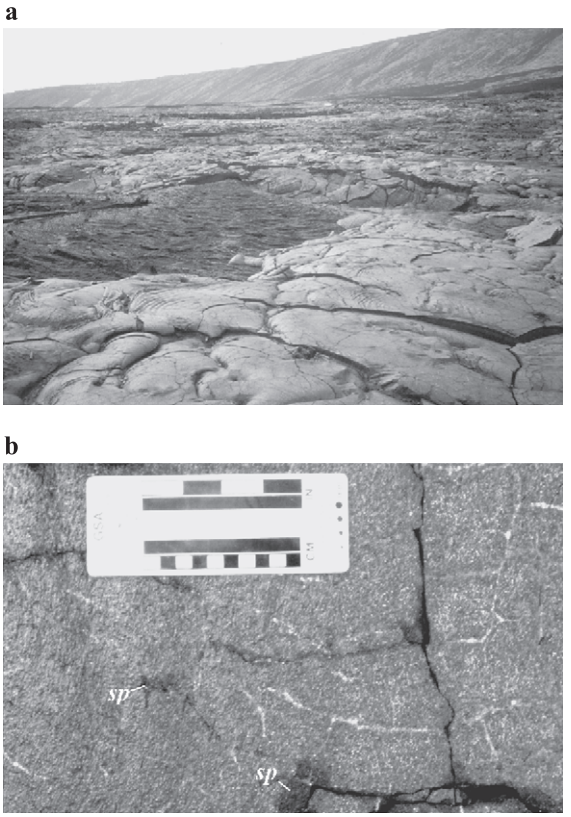

Fig. 8. Example of unit I pahoehoe at site 3.2.a. (a) Site overview, showing coalesced toes and small sheets in foreground overlying an older Mauna Ulu ropy channel. Fractures and offset crust that are evident in the photograph are interpreted to result from minor flow inflation. (b) Unit detail, showing a smooth, glassy, relatively non-vesicular surface; small areas displaying the spallation surface (*sp*) on which vesicles are exposed; small surficial cracks associated with a white surface coating or alteration; and dark fractures of the crust that are associated with cooling and minor flow inflation. Upper scale bar in inches, lower bar in centimeters.

local (decimeter-scale) areas that have larger knobs, these protrusions are more abundant and less bronzy. The surface crust lacks both vesicles and phenocrysts but in places displays the splotchy, orange-colored alteration (in portions of flat and ropy areas) and the white-colored coating (along small cracks). The spallation surface, representing ~5% of the exposure, displays ~25% vesicles (up to 3 mm, but typically 0.5 mm) and <1% phenocrysts (≤3 mm long). This unit I exposure was fed from a 4-m-long ropy-pahoehoe-surfaced channel (over a lava tube) and fed networks of toe lobes downflow. The site apparently experienced minor flow inflation as indicated by fractures in the unit surface and maximum local relief (fracture offset) of ~22 cm.

Site 6.1.a1 (~15 × 10 m) is shown in Fig. 9. It exhibits discrete pahoehoe toes that are transitional to coalesced toes at the site 6.1.a unit I exposure. The unit II toes are several decimeters to ~1 m in size, with larger toes tending to be more elongate. The surface crust displays bronze-colored, stretched glass filaments and dark knobs; vesicles are uncommon (<5%) and small (1–2 mm). Approximately half of the surface crust has been spalled (Fig. 9b), revealing a surface with more abundant vesicles (~30%) of the same size. Phenocrysts and surface coatings and alteration are absent. Inflation occurred, as manifested

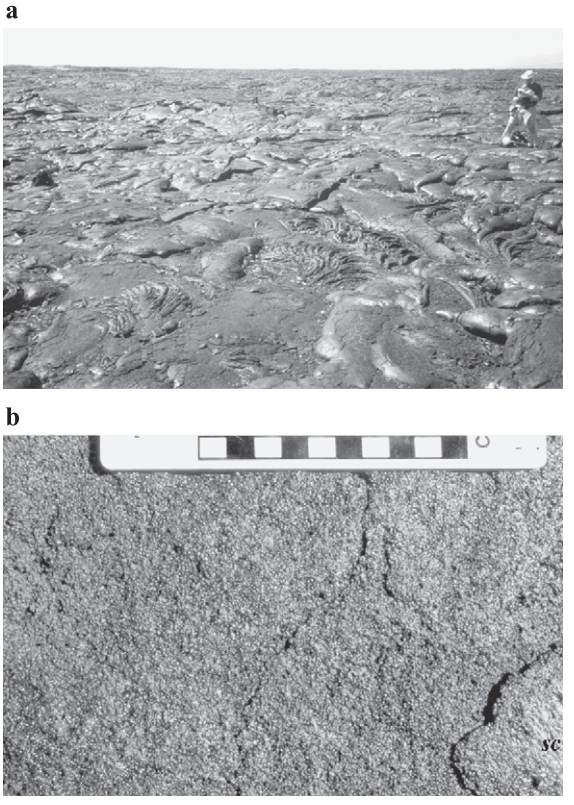

Fig. 9. Example of unit II pahoehoe at site 6.1.a1. (a) Site overview, showing discrete toes (near M. Ramsey) transitioning (to the left) to coalesced toes forming a unit I surface. (b) Unit detail, showing spallation surface with a small portion of the glassy surface crust at the lower right (*sc*). Scale bar in centimeters.

in a large tumulus from which squeeze-ups emanate (e.g. Walker, 1991).

The site 3.1.b (~ 15 × 30 m) unit III toes (Fig. 10) appear to be the youngest surface unit locally, fed as a breakout from the distal end of the site 3.1.c unit IV channel. Toes are decimeters to several meters in length; smaller toes tend to be smooth whereas larger toes tend to be ropy. The unit III surface crust is dark with a vitreous luster. The surface displays abundant (~ 40%), elongate vesicles that are 1–2 mm long. Olivine phenocrysts are present (<5%) and up to 3 mm long on the surface crust. Most of the surface crust has been spalled (90%), exposing a dark, highly vesicular (60%) surface. Vesicles are typically 1 mm across, but range up to 5 mm. Olivine phenocrysts make up ~ 10% of the spallation surface and are up to 2 mm long.

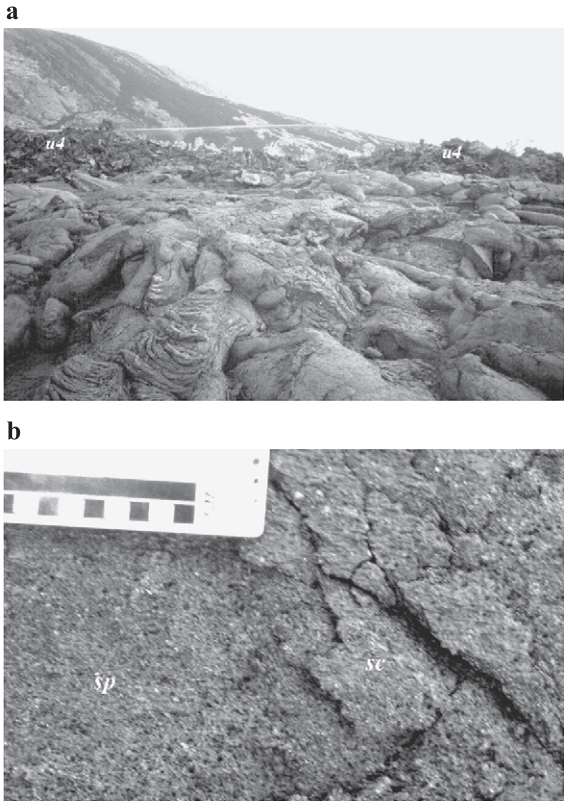

Fig. 10. Example of unit III pahoehoe at site 3.1.b. (a) Site overview, showing toes that are relatively thick, commonly ropy, and accumulate to form "centrally ridged" lobes (Crown and Baloga, 1999). Site 3.1.c unit IV exposure is visible as disrupted, dark plates in photo midground (*u4*); Chain of Craters Road is visible along the pali in the background. (b) Unit detail, showing rough surface crust (*sc*) and highly vesicular spallation surface (*sp*). Scale bar in centimeters.

Fig. 11. Example of unit IV pahoehoe at site 3.1.c. Unit overview shows disrupted surface displaying primary unit I and/or II textures in smooth and ropy plates with glassy surfaces, primary unit III textures in dark plates with rough surfaces, and ′a′a texture on clinkers.

The site 3.1.c (~ 75 × 45 m) unit IV channel (Fig. 11) is highly variable, including the following: slabs that display a flat, bronzy, stretched-glass unit I- and II-type surface texture; slabs with centimeter-scale compressional folds displaying glassy surfaces; slabs of overturned crust that are gray-brown and non-vesicular; reddish, vesicular ′a′a clinkers; and slabs displaying unit III-type surface crusts and spallation surfaces. Small pieces of wind-blown reticulite have accumulated in topographic lows across the unit surface.

6.2. Remote sensing characteristics of selected sites

Point (single-pixel) spectra for the four selected sites are shown in Fig. 12. These spectra do not display the simple relationships observed in the mean unit spectra (Figs. 4 and 5). Specifically, in the ASTER VNIR data, the pixel containing the unit III exposure at site 3.1.b has a higher reflectance at all three wavelengths than the other three site pixels. The unit I and IV sites (3.2.a and 3.1.c, respectively) display similar reflectance, and the unit II site (6.1.a1) has the lowest reflectance at all wavelengths. ASTER point emissivity spectra display the opposite trend of the mean emissivity trend—units III and IV

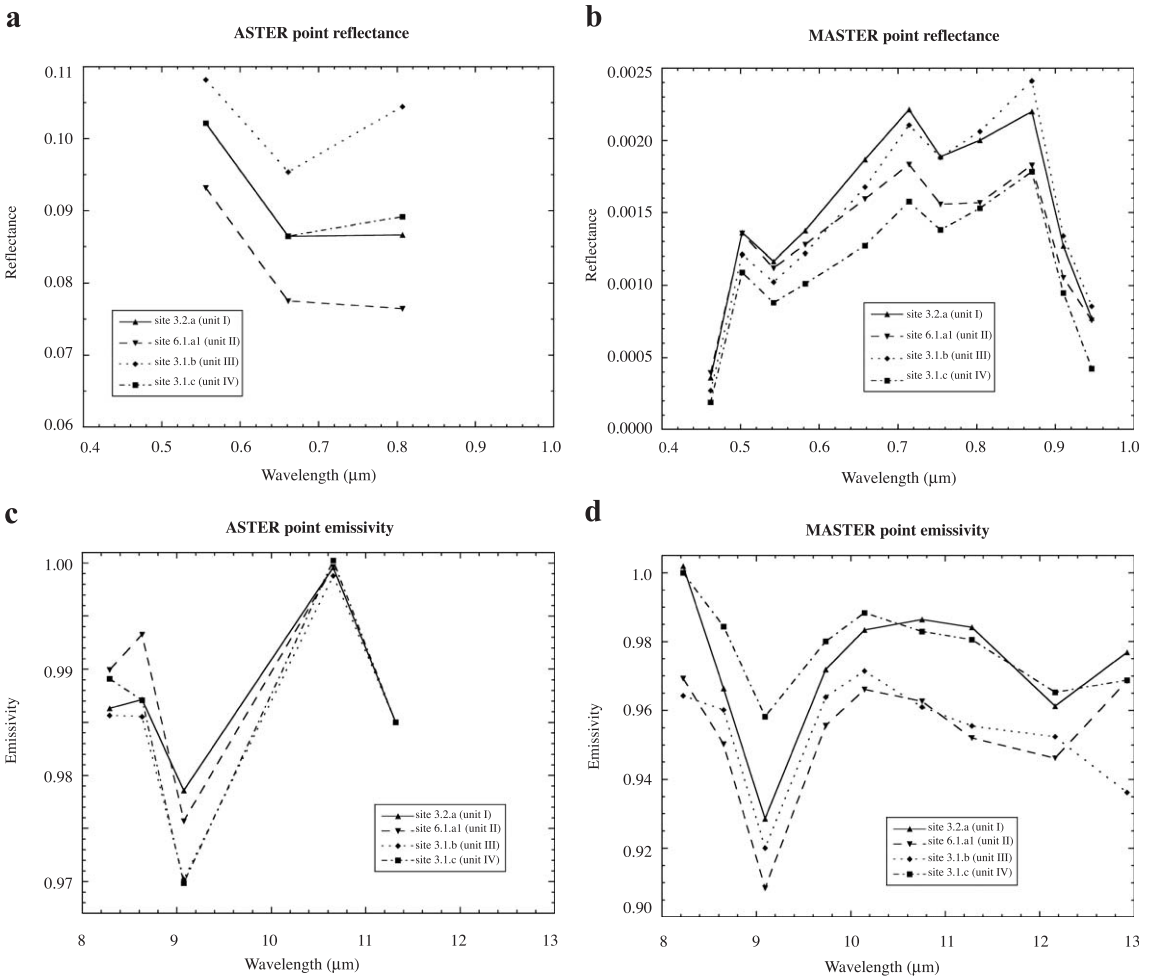

Fig. 12. Point spectra of the four selected sites (see Fig. 1 inset and Section 6.1 text). (a) ASTER VNIR-derived reflectance, bands 1 to 3. (b) MASTER VNIR-derived reflectance, bands 1 to 11. (c) ASTER TIR-derived emissivity, bands 10 to 14. (d) MASTER TIR-derived emissivity, bands 42 to 50.

display the most prominent 9.1-μm feature, followed by unit II and unit I. The MASTER VNIR data indicate that overall the unit I site is the brightest pixel of the four, followed by the unit III and II sites, and finally the unit IV site, although the progression is not consistent at all wavelengths. The MASTER point emissivity spectra also depart significantly from the mean spectra, which is reflected in the calculated site small-scale roughness (Fig. 7). Roughness of the selected sites does not show the simple increase from unit I to II to III to IV that is indicated by the field data and mean TIR-derived values. Additionally, the mean and point TIR-derived roughness values are significantly higher than field-based estimates of vesicularity.

6.3. Significance

The spectral data for individual sites diverges significantly from the trends established by mean unit data. The pahoehoe morphologies discussed herein (sheets, channels, and toes) are expressed within surface units of the Mauna Ulu flow field at the meter scale. Both the ASTER and MASTER pixels are much larger than this (≥ 15 and >10 m/pixel, respectively) and therefore typically sample

multiple surface units (i.e. mixed pixels). For example, the site 3.1.c unit IV exposure is adjacent to a kipuka of exposed pre-Mauna Ulu basalt. This pre-eruption surface is visibly much brighter than the Mauna Ulu basalt due to more extensive weathering of the surface (consistent with observations by Lockwood and Lipman (1987) of basalt weathering on Mauna Loa). Mixing of the pre-eruption surface with the unit IV surface within the pixel accounts for increased reflectance in the ASTER VNIR data and increased roughness in the MASTER TIR-derived data. Differences between the ASTER and MASTER VNIR point data are due, at least in part, to differences in the actual pixel footprints and may be amplified by small (<30 m) errors in coregistration. The ASTER and MASTER TIR data have very different spatial resolution, which causes even greater differences in derived emissivity and small-scale roughness. Mixed pixels cause point spectra to represent averaged values. This effect is illustrated in Fig. 7 in that roughness values derived from the remote sensing data are fairly constant for units I–III relative to those observed in the field, because the unit I and II sites are in pixels that include rougher surfaces and the unit III site is within a pixel that includes smoother surfaces. The TIR-derived roughness values are in most cases higher than the field-based vesicularity estimates, although no consistent difference in values is present (+51% to −3%). This indicates that small-scale roughness elements other than vesicles contribute to the emissivity spectra, such as observed millimeter-scale knobs and ridges and to a lesser extent small-scale surface fractures.

It has been documented that surficial coatings and alteration affect TIR signatures of basalt. For example, they can mask the 9.1-μm absorption feature if composed of hematite or palagonite (Fig. 2 of Kahle et al., 1988) or halite from sea spray (ASTER spectral library, http://speclib.jpl.nasa.gov/); alternatively, they may enhance the glass signature if composed of amorphous silica, although amorphous silica is not abundant on the Mauna Ulu flow field surface. Whereas observed surface coatings and alteration may affect emissivity spectra at locales, coatings and alteration are generally not areally extensive and, if present, do not appear to affect the separability of unit surfaces based on the mean spectra.

7. Discussion

Two dominant types of surface crusts have been analyzed using field observations and VNIR and TIR remote sensing data. Because Mauna Ulu surface units are typically smaller than pixels in ASTER and MASTER data, details of unit emplacement are generally not identifiable due to various mixtures of multiple units within a given pixel (i.e. mixed pixels), as discussed in Section 6. Characteristic unit spectra are better defined by increasing the ratio of signal from a surface unit to noise of other unit surfaces, accomplished by averaging a larger number of pixels as discussed in Sections 5.3–5.5. Thus, within the Mauna Ulu flow field, ASTER and MASTER datasets may be used to constrain the dominant surface unit over larger (multiple-pixel) areas as well as characterize gross changes that occur in the distribution of units within the flow field. Higher-resolution data are necessary to precisely map the units observed in the field (cf. Fig. 1c and d).

Several large-scale trends in emplacement are apparent within the Mauna Ulu flow field, based on synthesizing the field and remote sensing analyses presented herein. Surface-fed pahoehoe units (fountain-fed and shelly) are emplaced as large sheets, toes, and channels, and signify relatively high lava supply rates. ASTER and MASTER data indicate that the proximal pahoehoe surface units have VNIR and TIR spectral signatures that are similar to each other and relatively homogeneous at the scale of the data, except for the substantial chemical alteration immediately adjacent to the Mauna Ulu vent. The highly altered material nearest the vent is not distinguishable in the roughness data, presumably because the ASTER TIR data lack sufficient spatial resolution and the MASTER data have sufficient cloud cover to mask an alteration signature. Medial and distal portions of the flow field display ′a′a and tube-fed pahoehoe units I–IV. ′A′a exposures are more common in the medial zone than in the proximal zone, which may be partly due to the nature of the pahoehoe to ′a′a textural transition and partly due to burial by subsequent pahoehoe flows above Holei Pali. Tube-fed pahoehoe is emplaced as sheets, toes, and channels that display different small-scale surface characteristics due to differences in cooling, degassing, and crystal forma-

tion and settling. The small-scale roughness model indicates that the smoothest areally extensive surfaces within the Mauna Ulu flow field are located in interior portions (i.e. away from flow margins) of the medial region, with roughness increasing toward the flow field margins and increasing downflow. These effects are presumably caused by progressive downflow disruption of the lava flows and increased cooling of lava transported away from the master tubes, despite the limited cooling within the master tube system. Swanson (1973) indicated that lava flowing through the Mauna Ulu master tubes did not display measurable cooling downslope based on optical pyrometer measurements. Higher-precision measurements using glass geothermometry indicate cooling of typically <1 °C/km within the Pu′u ′O′ o master tube system (Helz et al., 2003). It is expected, however, that flow velocities decrease as lava is transported away from the main lava tube segments through smaller distributary lava tubes, due to decreased local supply within the tube system and increased friction along tube walls relative to the lava volume transported, which may increase the rate of heat loss relative to distance transported within a tube. Cooling within distributary tubes may be augmented by greater lava surface area to volume ratios, which promotes conductive cooling to the tube walls. Additionally, diminished flow can promote storage, which allows further cooling of the lava prior to emplacement. In this fashion, lava storage within distributary tubes may promote formation of unit III pahoehoe and dark, rough surface crusts. The distribution of this unit morphology and crust variety may therefore be used to delineate sites of subsurface storage and hence constrain the geometry of the lava tube system.

Crust spallation is a complicating factor for surface unit identification using both VNIR and TIR remote sensing data because it appears to be related both to lava flow characteristics during emplacement (such as flow viscosity) as well as post-emplacement unit modification (such as inflation). Significant variations in our field measurements show that spallation is not a simple function of morphologic form. In addition, the effects of inflation on surface crusts appear to be non-systematic, varying with extent and scale of flow inflation. For example, inflation of an individual pahoehoe toe can increase surface spall, whereas inflation of an entire flow unit may not significantly influence spall. Spallation darkens surface units by removing the smoothest, most reflective portion of the surface crust. TIR-derived emissivity data are responsive to variations in proportion of smooth glass vs. small-scale roughness elements (including vesicles, surface protuberances, etc.). The formation of surface roughness elements is related to flow emplacement processes, as well as the thermal and degassing histories of the lava. For example, vesicularity is a function of the initial gas content, gas loss at the vent, and gas exsolution and loss during transport and storage; small surface knobs appear to have been produced by vesicle deformation during crust formation. Spallation increases small-scale roughness by exposing increasingly vesicle-rich surfaces from beneath primary surface crusts.

8. Summary and conclusions

The Mauna Ulu flow field exhibits surface units displaying a range of morphologies and textures that result from differences in flow emplacement conditions, including four tube-fed pahoehoe units (I–IV), proximal surface-fed pahoehoe (shelly and fountain-fed), and ′a′a. Unit-scale primary morphologies, including lobes of pahoehoe toes, sheets, and channels, are indicative of local supply conditions from the vent (for surface-fed flows) or from lava tubes (for tube-fed flows). The analysis of Byrnes and Crown (2001) led to categorization of four varieties of tube-fed pahoehoe units in the medial portion of the flow field, defined on the basis of their dominant meter-scale morphology and the color of the surface crust. These pahoehoe units reflect differences in emplacement controlled primarily by local flow rate and unit remobilization, which are correlated with underlying topographic slopes. This categorization did not, however, provide a complete characterization of the flow field surface due to transitions between these units and the presence of additional units within other parts of the flow field. Analyses conducted herein have focused on new detailed characterizations of surface crusts to improve our understanding of surface units at Mauna Ulu.

Overall, the Mauna Ulu flow field surface is glassy and phenocryst poor. Characteristic variations related

to differences in emplacement processes between surface units are identifiable in both field and remotely sensed VNIR and TIR spectra. The wide range in characteristics observed in the field indicates that each of the units may be produced under a range of conditions, consistent with the gradational nature of the units observed within the flow field. Two dominant types of surface crusts have been characterized: a bronzy, smooth variety (associated with pahoehoe units I and II) and a dark, rough variety (associated with pahoehoe unit III). These two varieties of surface crusts are indicative of the state of the lava during emplacement, reflecting differences in cooling and crystallization related to lava transport and storage. The observed range of surface textures indicates that these two principal varieties are gradational, suggesting a continuous but bimodal distribution of lava histories, related to differences in cooling and crystallization during transport and storage within the distributary tube network.

Bronzy, smooth crust is associated with a full range of unit morphologies (i.e. toey lobes, sheets, and channels) and occurs in small, medium, and large surface units. This crust type is areally dominant within the flow field. In terms of Byrnes and Crown (2001), pahoehoe units I and II exhibit no distinct differences in surface crust characteristics, but rather reflect differences in local emplacement parameters, such as flow rate, topography, and inflation and coalescence. The bronzy, smooth crust, which comprises the majority of Mauna Ulu pahoehoe surfaces, is believed to represent lava that experienced negligible cooling and degassing prior to emplacement. Dark, rough crust typically is associated with small lava breakouts. These units are commonly associated with tumuli and channelized flows, however more extensive sheet-like exposures have been observed in a few localities. The small-scale properties of this variety of surface crust and the typical association of this crust with small lobes of unit III pahoehoe toes are consistent with low flow rate and high bulk viscosity during emplacement relative to the bronzy, smooth variety. Successive stages of dark lava breakouts emplacing rougher, more phenocryst-rich lava supports the interpretation that storage and cooling within the flow field controls the formation of lava displaying this surface crust variety.

These two varieties of surface crusts have different characteristic VNIR and TIR spectral properties, which have been identified by averaging many pixels. Flow field analysis using data that have pixels larger than the flow units can provide information on gross changes in lava emplacement within the flow field. Application of the methodology presented herein to flows in different settings may be used to better understand effects of eruption parameters (e.g. supply rate, eruption style) and setting (e.g. transport network, topography, cooling environment) on the emplacement of lava flow fields.

Acknowledgements

The assistance of Chris Eisinger with the MASTER atmospheric correction, Brian Banks with field observations, and Bill Harbert, Sarah B.Z. McElfresh, and Tamara Misner with image processing is greatly appreciated. Thanks also go to Darcy Hu of Hawai′i Volcanoes National Park for help with sample collection permits and Rosalind Helz for providing a preprint of her lava tube chapter. The manuscript benefited greatly from thorough reviews and additional assistance by Dave Sherrod and Scott Rowland. This research was supported by NASA grant NAG5-10561. This is PSI contribution #363.

Appendix A

Sites listed in Table A1 were geolocated by mapping unit margins using a Trimble dGPS receiver to achieve ~10 cm accuracy. Point locations listed herein approximate unit geometric centers, although in some cases are offset so that the point lies within the unit. Additional information concerning the sites is presented in the text and Table 1. Positions are reported in Eastings and Northings relative to a UTM zone 5 (North) projection, on a WGS84 spheroid. For convenience, latitude and longitude measurements are included, computed using the coordinate converter available at http://jeeep.com/details/coord/. Not all sites in which detailed field surface characterizations were made (Table 1) were precisely located. Some additional sites where observations were made

Table A1
Mauna Ulu study site locations

Site	Unit	Location	
		Easting, northing	Latitude, longitude
3.1.a	II	274152.5°E, 2135702.5°N	19°18.15′ N, 155°8.96′ W
3.1.b	III	274167.0°E, 2135682.0°N	19°18.14′ N, 155°8.95′ W
3.1.b1[a]	II	274162.0°E, 2135684.5°N	19°18.14′ N, 155°8.96′ W
3.1.c	IV	274148.5°E, 2135724.5°N	19°18.16′ N, 155°8.96′ W
3.1.c1[b]	II	274134.0°E, 2135747.0°N	19°18.18′ N, 155°8.97′ W
3.1.d	I	274152.0°E, 2135657.5°N	19°18.13′ N, 155°8.96′ W
3.2.a	I	274130.5°E, 2135587.0°N	19°18.09′ N, 155°8.97′ W
3.3.b	IV	274204.5°E, 2135497.5°N	19°18.04′ N, 155°8.93′ W
3.7	III	274902.0°E, 2136061.0°N	19°18.35′ N, 155°8.53′ W
3.9	III	274896.5°E, 2136003.5°N	19°18.32′ N, 155°8.54′ W
3.12	′a′a leveed channel	274976.5°E, 2135840.5°N	19°18.23′ N, 155°8.49′ W
4.2	III (tumulus)	273191.0°E, 2135503.0°N	19°18.04′ N, 155°9.51′ W
4.3	III	273241.0°E, 2135329.5°N	19°17.94′ N, 155°9.48′ W
4.4	III	273231.5°E, 2135347.5°N	19°17.95′ N, 155°9.48′ W
4.5	III	273251.0°E, 2135313.0°N	19°17.94′ N, 155°9.47′ W
4.13	III	273059.0°E, 2134343.5°N	19°17.41′ N, 155°9.57′ W
4.17	′a′a and IV	273012.5°E, 2134101.0°N	19°17.28′ N, 155°9.60′ W
5.1.a	II	268470.5°E, 2139543.0°N	19°20.19′ N, 155°12.23′ W
6.1.a	I and II	274436.5°E, 2133929.0°N	19°17.19′ N, 155°8.79′ W
6.2.a	P-type pahoehoe	274474.0°E, 2133868.5°N	19°17.16′ N, 155°8.76′ W
6.3.a	I	272427.5°E, 2133669.5°N	19°17.04′ N, 155°9.93′ W
6.3.b	III	272399.5°E, 2133706.0°N	19°17.06′ N, 155°9.95′ W
6.4.a	I	272435.0°E, 2133572.5°N	19°16.98′ N, 155°9.93′ W
6.5.a	I	272428.0°E, 2133519.0°N	19°16.96′ N, 155°9.93′ W
7.1.a[c]	I	272088.5°E, 2137709.5°N	19°19.23′ N, 155°10.15′ W
7.1.a[d]	II	271931.5°E, 2137661.0°N	19°19.20′ N, 155°10.24′ W
7.1.a[e]	III	271941.0°E, 2137664.5°N	19°19.20′ N, 155°10.24′ W
7.2.a	I	271851.0°E, 2138156.0°N	19°19.47′ N, 155°10.29′ W
7.3.a	I	271539.0°E, 2137380.5°N	19°19.04′ N, 155°10.46′ W
7.4.a	II	271387.0°E, 2137336.0°N	19°19.02′ N, 155°10.55′ W
7.5.a	IV	271441.5°E, 2137129.5°N	19°18.91′ N, 155°10.52′ W
7.6.a	I	271489.5°E, 2136942.5°N	19°18.81′ N, 155°10.49′ W
7.7.a	II	271628.0°E, 2136818.5°N	19°18.74′ N, 155°10.41′ W
7.8.a	IV	271526.0°E, 2136722.5°N	19°18.69′ N, 155°10.47′ W

[a] Inlier to site 3.1.b.
[b] Inlier to site 3.1.c.
[c] Contains site 7.1.aA.
[d] Contains site 7.1.aC.
[e] Contains site 7.1.aB.

but surface characterizations were not compiled are included (Table A1).

References

Byrnes, J.M., Crown, D.A., 2001. Relationships between pahoehoe surface units, topography, and lava tubes at Mauna Ulu Kilauea Volcano, Hawaii. J. Geophys. Res. 106, 2139–2151.

Byrnes, J.M., Crown, D.A., Ramsey, M.S., 2000. Thermal remote sensing characteristics of basaltic lava flow surface units: implications for flow field evolution. Lunar and Planetary Science XXXI, Abst. #1867. Lunar and Planetary Institute, Houston (CD-ROM).

Cashman, K.V., Kauahikaua, J.P., 1997. Reevaluation of vesicle distributions in basaltic lava flows. Geology 25, 419–422.

Crisp, J., Kahle, A.B., Abbott, E.A., 1990. Thermal infrared spectral character of Hawaiian basaltic glasses. J. Geophys. Res. 95, 21657–21669.

Crown, D.A., Baloga, S.M., 1999. Pahoehoe toe dimensions, mor-

phology, and branching relationships at Mauna Ulu Kilauea Volcano, Hawai′i. Bull. Volcanol. 61, 288–305.

Crown, D.A., Byrnes, J.M., Baloga, S.M., 1998. Scale-dependent characteristics of Mauna Ulu pahoehoe flows. Lunar and Planetary Science XXIX, Abst. #1376. Lunar and Planetary Institute, Houston (CD-ROM).

Crown, D.A., Baloga, S.M., Byrnes, J.M., 1999. Emplacement of pahoehoe flow fields: scale-dependent characteristics of Mauna Ulu flows. Lunar and Planetary Science XXX, Abst. #1379. Lunar and Planetary Institute, Houston (CD-ROM).

Crown, D.A., Byrnes, J.M., Ramsey, M.S., 2001. Mapping compound lava flow fields on planetary surfaces. EOS (Trans.-Am. Geophys. Union), (Suppl. 62) (P32D-0566).

Crown, D.A., Byrnes, J.M., Baloga, S.M., 2004. Scale-dependent characteristics of Mauna Ulu pahoehoe flows, in preparation.

Gillespie, A.R., Smith, M.O., Adams, J.B., Willis, S.C., 1990. Spectral mixture analysis of multispectral thermal infrared images. In: Abbott, E.A. (Ed.), Proc. Sec. Therm. Infrared Multispectral Scanner (TIMS) Workshop. JPL Publ., vol. 90-55, pp. 57–74.

Harris, A.J.L., Flynn, L.P., Kesthelyi, L., Mouginis-Mark, P.J., Rowland, S.K., Resing, J.A., 1998. Calculation of lava effusion rates from Landsat TM data. Bull. Volcanol. 60, 52–71.

Helz, R.T., Heliker, C., Hon, K., Mangan, M., 2003. Thermal efficiency of lava tubes in the Pu′u ′O′o-Kupaianaha eruption. In: Heliker, C.C., Swanson, D.A., Takahashi, T.J. (Eds.), The Pu′u ′O′o-Kupaianaha Eruption of Kilauea Volcano, Hawai′i: The First Twenty Years. U. S. Geol. Surv. Prof. Pap. 1676, 105–120.

Holcomb, R.T., 1976. Preliminary map showing products of eruptions, 1962–1974 from the Upper East Rift Zone of Kilauea Volcano, Hawaii. U.S. Geol. Surv. Misc. Field Studies, Map MF-811, scale 1:24,000.

Holcomb, R.T., 1987. Eruptive history and long-term behavior of Kilauea Volcano. In: Decker, R.W., Wright, T.L., Stauffer, P.H. (Eds.), Volcanism in Hawaii. U. S. Geol. Surv. Prof. Pap. 1350, 261–350.

Hon, K., Kauahikaua, J., Denlinger, R., Mackay, K., 1994. Emplacement and inflation of pahoehoe sheet flows: observations and measurements of active lava flows on Kilauea Volcano, Hawaii. Geol. Soc. Am. Bull. 106, 351–370.

Hook, S.J., Gabell, A.R., Green, A.A., Kealy, P.S., 1992. A comparison of techniques for extracting emissivity information from thermal infrared data for geologic studies. Remote Sens. Environ. 42, 123–135.

Hook, S.J., Myers, J.J., Thome, K.J., Fitzgerald, M., Kahle, A.B., 2001. The MODIS/ASTER airborne simulator (MASTER)—a new instrument for Earth science studies. Remote Sens. Environ. 76, 93–102.

Kahle, A.B., Alley, R.E., 1992. Separation of temperature and emittance in remotely sensed radiance measurements. Remote Sens. Environ. 42, 107–111.

Kahle, A.B., Gillespie, A.R., Abbott, E.A., Abrams, M.J., Walker, R.E., Hoover, G., Lockwood, J.P., 1988. Relative dating of Hawaiian lava flows using multispectral thermal infrared images: a new tool for geologic mapping of young volcanic terranes. J. Geophys. Res. 93, 15239–15251.

Kauahikaua, J., Sherrod, D.R., Cashman, K.V., Heliker, C., Hon, K., Mattox, T.N., Johnson, J.A., 2003. Hawaiian lava-flow dynamics during the Pu′u ′O′o-Kupaianaha eruption: a tale of two decades. In: Heliker, C.C., Swanson, D.A., Takahashi, T.J. (Eds.), The Pu′u ′O′o-Kupaianaha Eruption of Kilauea Volcano, Hawai′i: The First Twenty Years. U.S. Geol. Surv. Prof. Pap. 1676, 63–88.

Keszthelyi, L., Denlinger, R., 1996. The initial cooling of pahoehoe flow lobes. Bull. Volcanol. 58, 5–18.

Kruse, F.A., Kierein-Young, K.S., 1990. Mapping lithology and alteration in the northern Death Valley region, California and Nevada, with the Thermal Infrared Multispectral Scanner (TIMS). In: Abbott, E.A. (Ed.), Proc. Sec. Therm. Infrared Multispectral Scanner (TIMS) Workshop. JPL Publ., vol. 90-55, pp. 75–81.

Lockwood, J.P., Lipman, P.W., 1987. Holocene eruptive history of Mauna Loa Volcano. In: Decker, R.W., Wright, T.L., Stauffer, P.H. (Eds.), Volcanism in Hawaii. U. S. Geol. Surv. Prof. Pap. 1350, 509–535.

Mattox, T.N., Heliker, C., Kauahikaua, J., Hon, K., 1993. Development of the 1990 Kalapana flow field, Kilauea Volcano, Hawaii. Bull. Volcanol. 55, 407–413.

McBirney, A.R., 1993. Igneous Petrology. Jones and Bartlett, Boston.

Moore, J.G., Phillips, R.L., Grigg, R.W., Peterson, D.W., Swanson, D.A., 1973. Flow of lava into the sea, 1969–1971, Kilauea Volcano, Hawaii. Geol. Soc. Am. Bull. 84, 537–546.

Ondrusek, J., Christensen, P.R., Fink, J.H., 1993. Mapping the distribution of vesicular textures on silicic lavas using the thermal infrared multispectral scanner. J. Geophys. Res. 98, 15903–15908.

Peterson, D.W., Tilling, R.I., 1980. Transition of basaltic lava from pahoehoe to aa, Kilauea Volcano, Hawaii: field observations and key factors. J. Volcanol. Geotherm. Res. 7, 271–293.

Pieri, D., Abrams, D., 2004. ASTER watches the world's volcanoes: a new paradigm for volcanological observation from orbit. J. Volcanol. Geotherm. Res. 135, 13–28 (this issue).

Pinkerton, H., Sparks, R.S.J., 1976. The 1975 sub-terminal lavas, Mount Etna: a case history of the formation of a compound flow field. J. Volcanol. Geotherm. Res. 1, 167–182.

Polacci, M., Cashman, K.V., Kauahikaua, J.P., 1999. Textural characterization of the pahoehoe—′a′a transition in Hawaiian basalt. Bull. Volcanol. 60, 595–609.

Ramsey, M.S., Christensen, P.R., 1998. Mineral abundance determination: quantitative deconvolution of thermal emission spectra. J. Geophys. Res. 103, 577–596.

Ramsey, M.S., Dehn, J., 2004. Spaceborne observations of the 2000 Bezymianny, Kamchatka eruption: the integration of high-resolution ASTER data into near real-time monitoring using AVHRR. J. Volcanol. Geotherm. Res. 135, 127–146 (this issue).

Ramsey, M.S., Fink, J.H., 1997. Mapping vesicularity of Hawaiian lava flows via thermal infrared remote sensing. Abstr. Programs-Geol. Soc. Am., Cordilleran Sect. 29 (5), A58.

Ramsey, M.S., Fink, J.H., 1999. Estimating silicic lava vesicularity with thermal remote sensing: a new technique for volcanic mapping and monitoring. Bull. Volcanol. 61, 32–39.

Ramsey, M.S., Flynn, L.P., 2004. Strategies, insights, and the re-

cent advances in volcanic monitoring and mapping with data from the earth observing system. J. Volcanol. Geotherm. Res. 135, 1–11 (this issue).

Realmuto, V.J., 1990. Separating the effects of temperature and emissivity: emissivity spectrum normalization. In: Abbott, E.A. (Ed.), Proc. Sec. Therm. Infrared Multispectral Scanner (TIMS) Workshop. JPL Publ., vol. 90-55, pp. 31–36.

Realmuto, V.J., Hon, K., Kahle, A.B., Abbott, E.A., Pieri, D.C., 1992. Multispectral thermal infrared mapping of the 1 October 1988 Kupaianaha flow field, Kilauea Volcano, Hawaii. Bull. Volcanol. 55, 33–44.

Rowland, S.K., Walker, G.P.L., 1987. Toothpaste lava: characteristics and origin of a lava structural type transitional between pahoehoe and aa. Bull. Volcanol. 49, 631–641.

Rowland, S.K., Walker, G.P.L., 1990. Pahoehoe and aa in Hawaii: volumetric flow rate controls the lava structure. Bull. Volcanol. 52, 615–628.

Ruff, S.W., Christensen, P.R., Barbera, P.W., Anderson, D.L., 1997. Quantitative thermal emission spectroscopy of minerals: a laboratory technique for measurement and calibration. J. Geophys. Res. 102, 14899–14913.

Salisbury, J.W., D'Aria, D.M., 1992. Emissivity of terrestrial materials in the 8–14 μm atmospheric window. Remote Sens. Environ. 42, 83–106.

Swanson, D.A., 1973. Pahoehoe flows from the 1969–1971 Mauna Ulu eruption, Kilauea Volcano, Hawaii. Geol. Soc. Am. Bull. 84, 615–626.

Swanson, D.A., Duffield, W.A., Jackson, D.B., Peterson, D.W., 1979. Chronological narrative of the 1969–1971 Mauna Ulu eruption of Kilauea Volcano, Hawai'i. U. S. Geol. Surv. Prof. Pap. 1056, 1–55.

Thomson, J.L., Salisbury, J.W., 1993. The mid-infrared reflectance of mineral mixtures (7–14 μm). Remote Sens. Environ. 45, 1–13.

Tilling, R.I., Christiansen, R.L., Duffield, W.A., Endo, E.T., Holcomb, R.T., Koyanagi, R.Y., Peterson, D.W., Unger, J.D., 1987. The 1972–1974 Mauna Ulu eruption, Kilauea Volcano: an example of quasi-steady-state magma transfer. In: Decker, R.W., Wright, T.L., Stauffer, P.H. (Eds.), Volcanism in Hawaii. U. S. Geol. Surv. Prof. Pap. 1350, 405–469.

Vincent, R.K., Thomson, F., 1972. Spectral compositional imaging of silicate rocks. J. Geophys. Res. 77, 2465–2472.

Vincent, R.K., Thomson, F., Watson, K., 1972. Recognition of exposed quartz sand and sandstone by two-channel infrared imagery. J. Geophys. Res. 77, 2473–2477.

Walker, G.P.L., 1972. Compound and simple lava flows and flood basalts. Bull. Volcanol. 35, 579–590.

Walker, G.P.L., 1991. Structure, and origin by injection of lava under surface crust, of tumuli, "lava rises", "lava-rise pits", and "lava-inflation clefts" in Hawaii. Bull. Volcanol. 53, 546–558.

Walter, L.S., Salisbury, J.W., 1989. Spectral characterization of igneous rocks in the 8- to 12-μm region. J. Geophys. Res. 94, 9203–9213.

Wilmoth, R.A., Walker, G.P.L., 1993. P-type and S-type pahoehoe: A study of vesicle distribution patterns in Hawaiian lava flows. J. Volcanol. Geotherm. Res. 55, 129–142.

Yamaguchi, Y., Kahle, A.B., Tsu, H., Kawakami, T., Pniel, M., 1998. Overview of Advanced Spaceborne Thermal Emission Reflectance Radiometer. IEEE Trans. Geosci. Remote Sens. 36, 1062–1071.